

## 5.1: Ocean Circulation Models and Modeling

Stephen.Griffies@noaa.gov  
NOAA/Geophysical Fluid Dynamics Laboratory  
Princeton, USA

Anne.Marie.Treguier@ifremer.fr  
Laboratoire de Physique des Océans, LPO  
Brest, France

Draft from May 24, 2013

### 1 **5.1.1. Scope of this chapter**

2 We focus in this chapter on numerical models used to understand and predict large-  
3 scale ocean circulation, such as the circulation comprising basin and global scales. It  
4 is organized according to two themes, which we consider the “pillars” of numerical  
5 oceanography. The first addresses physical and numerical topics forming a foundation  
6 for ocean models. We focus here on the science of ocean models, in which we ask  
7 questions about fundamental processes and develop the mathematical equations for  
8 ocean thermo-hydrodynamics. We also touch upon various methods used to represent  
9 the continuum ocean fluid with a discrete computer model, raising such topics as the  
10 finite volume formulation of the ocean equations; the choice for vertical coordinate;  
11 the complementary issues related to horizontal gridding; and the pervasive questions  
12 of subgrid scale parameterizations. The second theme of this chapter concerns the  
13 applications of ocean models, in particular how to design an experiment and how to  
14 analyze results. This material forms the basis for ocean modeling, with the aim being  
15 to mechanistically describe, interpret, understand, and predict emergent features of the  
16 simulated, and ultimately the observed, ocean.

### 17 **5.1.2. Physical and numerical basis for ocean models**

18 As depicted in Figure 5.1.1, the ocean experiences a wide variety of boundary in-  
19 teractions and possesses numerous internal physical processes. Kinematic constraints  
20 on the fluid motion are set by the geometry of the ocean domain, and by assuming  
21 each fluid parcel conserves mass, save for the introduction of mass across the ocean  
22 surface (i.e., precipitation, evaporation, river runoff), or bottom (e.g., crustal vents).  
23 Dynamical interactions are described by Newton’s Laws, in which the acceleration of  
24 a continuum fluid parcel is set by forces acting on the parcel. The dominant forces  
25 in the ocean interior are associated with pressure, the Coriolis force, gravity, and to a  
26 lesser degree friction. Boundary forces arise from interactions with the atmosphere,  
27 cryosphere, and solid earth, with each interaction generally involving buoyancy and  
28 momentum exchanges. Material budgets for tracers, such as salt and biogeochemical  
29 species, as well as thermodynamic tracers such as heat or enthalpy, are affected by  
30 circulation, mixing from turbulent processes, surface and bottom boundary fluxes, and  
31 internal sources and sinks especially for biogeochemical tracers (see Chapter 5.7).

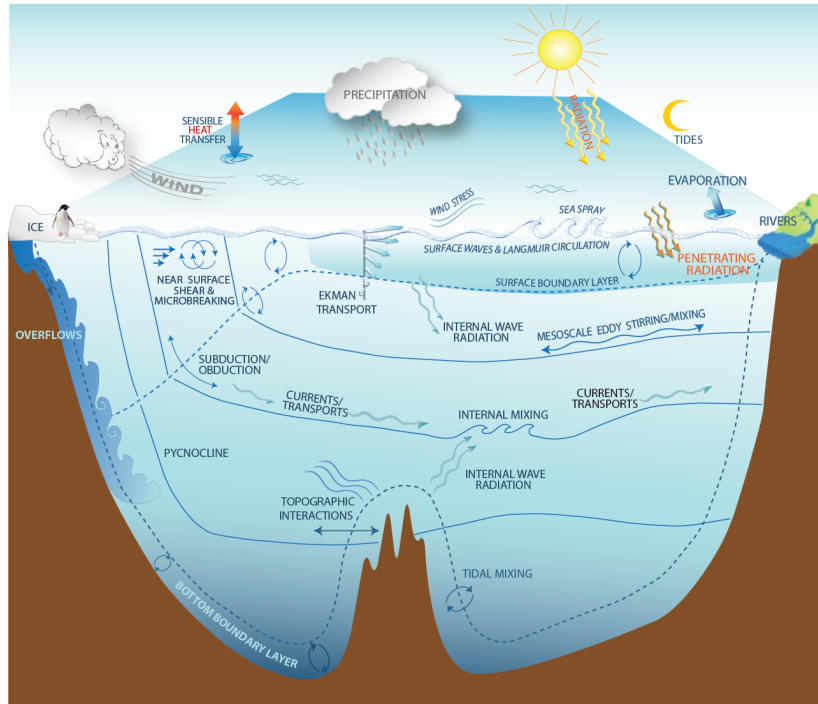


Figure 5.1.1: Understanding and quantifying the ocean’s role in the earth system, including coastal, regional, and global phenomena, involves a variety of questions related to how physical processes impact the movement of tracers (e.g., heat, salt, carbon, nutrients) and momentum across the ocean boundaries and within the ocean interior. The ocean interacts with the variety of earth system components, including the atmosphere, sea ice, land ice shelves, rivers, and the solid earth lower boundary. Ocean processes transport material between the ventilated surface boundary layer and the ocean interior. When in the interior, it is useful to characterize processes according to whether they transport material across density surface (dianeutrally) or along neutral directions (epineutrally). In this figure we illustrate the turbulent air-sea exchanges and upper ocean wave motions (including wave breaking and Langmuir circulations); subduction/obduction which exchanges material between the boundary layer and interior; gyre-scale, mesoscale, and submesoscale transport that largely occurs along neutral directions; high latitude convective and downslope exchange; and mixing induced by breaking internal gravity waves energized by winds and tides. Missing from this schematic include mixing due to double diffusive processes (Schmitt (1994)) and nonlinear equation of state effects (Chapter 3.2). Nearly all such processes are subgrid scale for present day global ocean climate simulations. The formulation of sensible parameterizations, including schemes that remain relevant under a changing climate (e.g., modifications to stratification and boundary forcing), remains a key focus of oceanographic research efforts, with Chapters 3.3 and 3.4 in this volume detailing many issues.

#### 5.1.2.1. SCALES OF MOTION

The ocean’s horizontal gyre and overturning circulations occupy nearly the full extent of ocean basins ( $10^3$  km to  $10^4$  km in horizontal extent and roughly 4 km in depth on average), with typical recirculation times for the horizontal gyres of decadal, and overturning time scales of millennial. The ocean microscale is on the order of  $10^{-3}$  m, and it is here that mechanical energy is transferred to internal energy through

38 Joule heating. The microscale is set by the *Kolmogorov length*

$$L_{\text{Kol}} = (\nu^3/\epsilon)^{1/4}, \quad (5.1.1)$$

39 where  $\nu \approx 10^{-6} \text{ m}^2 \text{ s}^{-1}$  is the molecular kinematic viscosity for water, and  $\epsilon$  is the  
40 energy dissipation rate. In turn, molecular viscosity and the Kolmogorov length imply  
41 a time scale  $T = L^2/\nu \approx 1 \text{ sec}$ .

42 Consider a direct numerical simulation of ocean climate, where all space and time  
43 scales between the Kolmogorov scale and the global scale are explicitly resolved by  
44 the simulation. One second temporal resolution over a millennial time scale climate  
45 problem requires more than  $3 \times 10^{10}$  time steps of the model equations. Resolving  
46 space into cubes of dimension  $10^{-3} \text{ m}$  for an ocean with volume roughly  $1.3 \times 10^{18} \text{ m}^3$   
47 requires  $1.3 \times 10^{27}$  discrete grid cells, which is roughly  $10^4$  larger than Avogadro's  
48 Number. These numbers far exceed the capacity of any computer, thus necessitating  
49 approximated or truncated descriptions for practical ocean simulations, and further-  
50 more promoting the central importance of subgrid scale parameterizations.

#### 51 5.1.2.2. THERMO-HYDRODYNAMIC EQUATIONS FOR A FLUID PARCEL

52 As a starting point for developing ocean model equations, we consider the thermo-  
53 hydrodynamic equations for an infinitesimal seawater parcel. Some of this material is  
54 standard from geophysical fluid dynamics as applied to the ocean (e.g., see books such  
55 as Gill (1982), Pedlosky (1987), Vallis (2006), Olbers et al. (2012)), so the presentation  
56 here will be focused on setting the stage for later discussions.

#### 57 **Mass conservation for seawater and trace constituents**

58 When formulating the tracer and dynamical equations for seawater, it is convenient  
59 to focus on a fluid parcel whose mass is constant. Writing the mass as  $M = \rho dV$ , with  
60  $dV$  the parcel's infinitesimal volume and  $\rho$  the *in situ* density, parcel mass conservation  
61  $dM/dt = 0$  yields the continuity equation

$$\frac{d\rho}{dt} = -\rho \nabla \cdot \mathbf{v}. \quad (5.1.2)$$

62 The three-dimensional velocity of the parcel is the time derivative of its position,  $\mathbf{v} =$   
63  $d\mathbf{x}/dt$ , and the horizontal and vertical components are written  $\mathbf{v} = (\mathbf{u}, w)$ . Transforming  
64 this parcel or material Lagrangian expression into a fixed space or Eulerian perspective  
65 leads to the equivalent form

$$\frac{\partial \rho}{\partial t} = -\nabla \cdot (\rho \mathbf{v}), \quad (5.1.3)$$

66 where we related the material time derivative to the Eulerian time derivative through

$$\frac{d}{dt} = \partial_t + \mathbf{v} \cdot \nabla. \quad (5.1.4)$$

67 Seawater is comprised of fresh water along with a suite of matter constituents such  
68 as salt, nutrients, and biogeochemical elements and compounds. The tracer concen-  
69 tration,  $C$ , which is the mass of trace matter within a seawater parcel per mass of the

70 parcel, is affected through the convergence of a tracer flux plus a potentially nonzero  
 71 source/sink term  $\mathcal{S}^{(C)}$  (sources and sinks are especially important for describing bio-  
 72 geochemical tracers; Chapter 5.7)

$$\rho \frac{dC}{dt} = -\nabla \cdot \mathbf{J}^{(C)} + \rho \mathcal{S}^{(C)}. \quad (5.1.5)$$

73 The canonical form of the tracer flux is associated with isotropic downgradient molec-  
 74 ular diffusion

$$\mathbf{J}_{\text{molecular}}^{(C)} = -\rho \kappa \nabla C, \quad (5.1.6)$$

75 where  $\kappa > 0$  is a kinematic molecular diffusivity with units of length times a velocity,  
 76 and  $\rho \kappa$  is the corresponding dynamic diffusivity. For large-scale ocean models, the  
 77 tracer flux  $\mathbf{J}^{(C)}$  is modified according to the parameterization of various unresolved  
 78 physical processes (see Chapters 3.3 and 3.4).

79 The Eulerian perspective converts the material time derivative into a local Eulerian  
 80 time derivative plus advection  $\rho (\partial_t + \mathbf{v} \cdot \nabla) C = -\nabla \cdot \mathbf{J}^{(C)} + \rho \mathcal{S}^{(C)}$ . Combining this  
 81 advective-form tracer equation with the seawater mass equation (5.1.3) leads to the  
 82 Eulerian flux-form of the tracer equation

$$\partial_t (\rho C) = -\nabla \cdot (\rho \mathbf{v} C + \mathbf{J}^{(C)}) + \rho \mathcal{S}^{(C)}. \quad (5.1.7)$$

83 Setting the tracer concentration to a uniform constant in the tracer equation (5.1.7) re-  
 84 covers the mass continuity equation (5.1.3), where we assumed there to be no seawater  
 85 mass source, and the tracer flux  $\mathbf{J}^{(C)}$  vanishes with the concentration constant (e.g., see  
 86 Section II.2 of DeGroot & Mazur (1984), Section 8.4 of Chaikin & Lubensky (1995),  
 87 or Section 3.3 of Müller (2006)). This connection between the tracer equation and the  
 88 seawater mass continuity equation is sometimes referred to as a *compatibility condition*  
 89 (see Griffies et al. (2001) or Chapter 12 of Griffies (2004)). Equivalently, requiring  
 90 that the tracer equation maintain a uniform tracer unchanged in the absence of bound-  
 91 ary fluxes is sometimes referred to as *local* tracer conservation, which is a property  
 92 required for conservative numerical algorithms. The flux-form in equation (5.1.7) is  
 93 used in Section 5.1.2.4 as the basis for developing finite volume equations for a region  
 94 of seawater.

### 95 **Conservative temperature and *in situ* density**

96 As detailed by McDougall (2003), potential enthalpy provides a useful measure of  
 97 heat in a seawater parcel (see also Chapter 3.2). Conservative temperature,  $\Theta$ , is the  
 98 potential enthalpy divided by a constant heat capacity. According to the First Law of  
 99 Thermodynamics, it satisfies, to an extremely good approximation, a scalar conserva-  
 100 tion equation directly analogous to material tracers

$$\rho \frac{d\Theta}{dt} = -\nabla \cdot \mathbf{J}^{(\Theta)}. \quad (5.1.8)$$

101 This equation, or its Eulerian form, are termed “conservative” since the net heat content  
 102 in a region is impacted only through fluxes passing across the boundary of that region  
 103 (see Chapter 5.7 for more discussion of conservative and non-conservative tracers).

104 In fact, there are actually nonzero source terms that are neglected in equation (5.1.8),  
 105 so that conservative temperature is not precisely “conservative”. However, McDougall  
 106 (2003) noted that these omitted source terms are negligible, as they are about 100 times  
 107 smaller than those source terms omitted when considering potential temperature,  $\theta$ , to  
 108 be a conservative scalar. It is for this reason that IOC et al. (2010) recommend the use  
 109 of conservative temperature,  $\Theta$ , as a means to measure the heat of a seawater parcel.

110 The equation of state, which provides an empirical expression for the *in situ* density  
 111  $\rho$ , is written as a function of conservative temperature, salinity, and pressure

$$\rho = \rho(\Theta, S, p). \quad (5.1.9)$$

112 Note that the equation of state as derived in IOC et al. (2010) is written in terms of the  
 113 Gibb’s thermodynamic potential, thus making it self-consistent with other thermody-  
 114 namic properties of seawater. Based on this connection, efforts are underway to update  
 115 ocean model codes and analysis methods towards the recommendations of IOC et al.  
 116 (2010).

### 117 Momentum equation

118 Newton’s Second Law of Motion applied to a continuum fluid in a rotating frame  
 119 of reference leads to the equation describing the evolution of linear momentum per  
 120 volume of a fluid parcel

$$\rho \left( \frac{d}{dt} + 2 \boldsymbol{\Omega} \wedge \right) \mathbf{v} = -\rho \nabla \Phi + \nabla \cdot (\boldsymbol{\tau} - \mathbf{I} p). \quad (5.1.10)$$

121 The momentum equation (5.1.10) encapsulates nearly all the phenomena of ocean and  
 122 atmospheric fluid mechanics. Such wide applicability is a testament to the power of  
 123 classical mechanics to describe observed natural phenomena. The terms in the equation  
 124 are the following.

- 125 • ACCELERATION: When considering fluid dynamics on a flat space, the acceleration  
 126 times density,  $\rho \, d\mathbf{v}/dt$ , takes the following Eulerian flux-form

$$\rho \frac{d\mathbf{v}}{dt} = \frac{\partial(\rho \mathbf{v})}{\partial t} + \nabla \cdot (\rho \mathbf{v} \mathbf{v}) \quad \text{flat space}, \quad (5.1.11)$$

127 which is directly analogous to the flux-form tracer equation (5.1.7). However, for  
 128 fluid dynamics on a curved surface such as a sphere, the acceleration picks up  
 129 an extra source-like term that is associated with curvature of the surface. When  
 130 using locally orthogonal coordinates to describe the motion, acceleration takes  
 131 the form (see Section 4.4.1 of Griffies (2004))

$$\rho \frac{d\mathbf{v}}{dt} = \frac{\partial(\rho \mathbf{v})}{\partial t} + \nabla \cdot (\rho \mathbf{v} \mathbf{v}) + \mathcal{M}(\hat{\mathbf{z}} \wedge \rho \mathbf{v}) \quad \text{sphere}. \quad (5.1.12)$$

132 For spherical coordinates,  $\mathcal{M} = (u/r) \tan \phi$ , with  $\phi$  the latitude and  $r$  the radial  
 133 position. At latitude  $\phi = 45^\circ$  with  $r \approx 6.37 \times 10^6 \text{ m}$ , and for a zonal current of  
 134  $u = 1 \text{ m s}^{-1}$ ,  $\mathcal{M} \approx 10^{-3} f$ , where

$$f = 2 \boldsymbol{\Omega} \sin \phi \quad (5.1.13)$$

is the Coriolis parameter (see below). Hence,  $\mathcal{M}$  is generally far smaller than the inertial frequency,  $f$ , determined by the Earth's rotation, except near the equator where  $f$  vanishes.

The nonlinear self-advective transport term  $\rho \mathbf{v} \cdot \nabla \mathbf{v}$  contributing to the acceleration (see equation (5.1.12)) accounts for the rich variety of nonlinear and cross-scale turbulent processes that pervade the ocean. At the small scales (hundreds of metres and smaller), such processes increase three-dimensional gradients of tracer and velocity through straining and filamentation effects, and in so doing increase diffusive fluxes. In turn, tracer variance and kinetic energy cascade to the small scales through the effects of three-dimensional turbulence (*direct cascade*), and are dissipated at the microscale (millimetres) by molecular viscosity and diffusivity. At the larger scales where vertical stratification and quasi-geostrophic dynamics dominates (Chapter 4.1), kinetic energy preferentially cascades to the large scales (*inverse cascade*) as in two-dimensional fluid dynamics, whereas tracer variance continues to preferentially cascade to the small scales. Such cascade processes are fundamental to how energy and tracer variance are transferred across the many space-time scales within the ocean fluid.

- **CORIOLIS FORCE:** Angular rotation of the earth about the polar axis, measured by  $\mathbf{\Omega}$ , leads to the Coriolis force per volume,  $2\rho \mathbf{\Omega} \wedge \mathbf{v}$ . The locally horizontal component to the rotation vector,  $f^* = 2\mathbf{\Omega} \cos \phi$ , can induce *tilted convection* that causes convecting plumes to deflect laterally (Denbo & Skillingstad (1996), Wirth & Barnier (2006, 2008)). Another effect was noted by Stewart & Dellar (2011), who argue for the importance of  $f^*$  in cross-equatorial flow of abyssal currents. However, hydrostatic primitive equation ocean models, which are the most common basis for large-scale models of the ocean, retain only the local vertical component of the earth's rotation, and thus approximate the Coriolis Force according to

$$2\rho \mathbf{\Omega} \wedge \mathbf{v} \approx \hat{\mathbf{z}} f \wedge (\rho \mathbf{v}), \quad (5.1.14)$$

where  $f$  (equation (5.1.13)) is termed the Coriolis parameter. Marshall et al. (1997) provides a discussion of this approximation and its connection to hydrostatic balance. It is this form of the Coriolis force that gives rise to many of the characteristic features of geophysical fluid motions, such as Rossby waves, Kelvin waves, western boundary currents, and other large-scale features (Chapter 4.1).

- **GRAVITATIONAL FORCE:** The gravitational potential,  $\Phi$ , is commonly approximated in global circulation models as a constant gravitational acceleration,  $g$ , times the displacement,  $z$ , from resting sea level or the surface ocean geopotential (geoid),

$$\Phi \approx g z. \quad (5.1.15)$$

However, the geopotential must be considered in its more general form when including astronomical tide forcing and/or changes to the geoid due to rearrangements of mass; e.g., melting land ice such as in the studies of Mitrovica et al. (2001) and Kopp et al. (2010).

- **FRICTIONAL STRESSES AND PRESSURE:** The symmetric second order deviatoric stress tensor,  $\tau$ , accounts for the transfer of momentum between fluid parcels due to shears, whereas  $p$  is the pressure force acting normal to the boundary of the parcel, with  $\mathbf{I}$  the unit second order tensor. At the microscale, frictional stresses are parameterized by molecular diffusive fluxes in the same way as for tracers in equation (5.1.6), with this parameterization based on analogy with the kinetic theory of gases (e.g., section 12.3 of Reif (1965)). Vertical stresses in the ocean interior are thought to be reasonably well parameterized in this manner for large-scale ocean models, with the eddy viscosity far larger than molecular viscosity due to momentum mixing by unresolved eddy processes. In contrast, there is no consensus on how to represent lateral frictional stress in large-scale ocean models, with modelers choosing lateral friction based on empirical (i.e., “tuning”) perspectives (Part 5 in Griffies (2004), as well as Jochum et al. (2008) and Fox-Kemper & Menemenlis (2008) for further discussion). In Section 5.1.2.6, we have more to say about certain issues involved with setting lateral friction in models.

#### Comments on the parcel equations

The mass conservation equation (5.1.2), tracer equation (5.1.5), conservative temperature equation (5.1.8), equation of state (5.1.9), momentum equation (5.1.10), and boundary conditions (Section 5.1.2.4), are the basic building blocks for a mathematical physics description of ocean thermo-hydrodynamics. However, these equations alone do not provide an algorithm for numerical simulations. Indeed, we know of no algorithm, much less a working numerical code, based on a realistic nonlinear equation of state for a mass conserving and non-hydrostatic ocean. Instead, various approximations are made, either together or separately, that have proven useful for developing numerical ocean model algorithms.

#### 5.1.2.3. APPROXIMATION METHODS

Three general approaches to approximation, or truncation, are employed in computational fluid dynamics, and we outline here these approaches as used for ocean models.

#### Coarse grid and realistic large-scale domain

One approach is to coarsen the space and time resolution used by the discrete grid forming the basis for the numerical simulation. By removing scales smaller than the grid, the truncated system carries less information than the continuum. Determining how the resolved scales are affected by the unresolved scales is fundamental to the science of ocean models: this is the parameterization problem (Section 5.1.2.5).

#### Refined grid and idealized small domain

A complementary approach is to configure a small space-time domain so as to maintain the very fine space and time resolution set by either molecular viscosity and diffusivity (direct numerical simulation (DNS)), or somewhat larger eddy viscosity and diffusivity (large eddy simulation (LES)). These simulations are necessarily idealized

both because of their small domain and the associated need to include idealized boundary conditions. Both DNS and LES are important for process studies aimed at understanding the mechanisms active in fine scale features of the ocean. Insights gained via DNS and LES have direct application to the development of subgrid scale parameterizations used in large-scale models. Large-scale simulations that represent a wide range of mesoscale and submesoscale eddies (e.g., finer than 1 km grid spacing) share much in common with LES (Fox-Kemper & Menemenlis, 2008). Such simulations will conceivably be more common for global climate scales within the next one or two decades, as computational power increases.

#### Filtering the continuum equations: hydrostatic approximation

A third truncation method filters the continuum equations by truncating the fundamental modes of motion admitted by the equations. This approach reduces the admitted motions and reduces the space-time scales required to simulate the system.

The hydrostatic approximation is a prime example of mode filtering used in large-scale modeling. Here, the admitted vertical motions possess far less kinetic energy than horizontal motions, thus rendering a simplified vertical momentum balance where the weight of fluid above a point in the ocean determines the pressure at that point

$$\frac{\partial p}{\partial z} = -\rho \frac{\partial \Phi}{\partial z} \quad \text{hydrostatic balance.} \quad (5.1.16)$$

Since vertical convective motion involves fundamentally non-hydrostatic dynamics (Marshall & Schott, 1999), hydrostatic primitive equation models must parameterize these effects (Klinger et al., 1996). Although the hydrostatic approximation is ubiquitous in large scale ocean modeling (for scales larger than roughly 1 km), there are many process studies that retain non-hydrostatic dynamics, with the MIT general circulation model (MITgcm) a common publicly available code used for such studies (Marshall et al., 1997).

#### Filtering the continuum equations: oceanic Boussinesq approximation

*In situ* density in the large-scale ocean varies by a relatively small amount, with a 5% variation over the full ocean column mostly due to compressibility. Furthermore, the dynamically relevant horizontal density variations are on the order of 0.1%. These observations motivate the *oceanic Boussinesq approximation*.

As detailed in Section 9.3 of Griffies & Adcroft (2008), the first step to the oceanic Boussinesq approximation applies a linearization to the momentum equation by removing the nonlinear product of density times velocity, in which the product  $\rho \mathbf{v}$  is replaced by  $\rho_o \mathbf{v}$ , where  $\rho_o$  is a constant Boussinesq reference density. However, one retains the *in situ* density dependence of the gravitational potential energy, and correspondingly it is retained for computing pressure. The second step considers the mass continuity equation (5.1.3), where the three-dimensional flow is incompressible to leading order

$$\nabla \cdot \mathbf{v} = 0 \quad \text{volume conserving Boussinesq approximation.} \quad (5.1.17)$$

This step filters acoustic modes (i.e., sound waves), if they are not already filtered by making the hydrostatic approximation.



As revealed by the mass conservation equation (5.1.2), a nontrivial material evolution of *in situ* density requires a divergent velocity field. However, a divergent velocity field is unresolved in oceanic Boussinesq models. Not resolving the divergent velocity field does not imply this velocity vanishes. Indeed, the oceanic Boussinesq approximation retains the dependence of density on pressure (or depth), temperature, and salinity (equation (5.1.9)), thus avoiding any assumption regarding the fluid properties. In turn, such models allow for a consistent material evolution of *in situ* density, with this evolution critical for representing the thermohaline induced variations in density (and hence pressure) that are key drivers of the large scale ocean circulation (Chapter 4.1).

An element missing from Boussinesq ocean models concerns the calculation of global mean sea level. Greatbatch (1994) noted that the accumulation of seawater compressibility effects over an ocean column leads to meaningful systematic changes in global sea level when, for example, the ocean is heated. These global steric effects must therefore be added *a posteriori* to a Boussinesq simulation of sea level to provide a meaningful measure of global sea level changes associated with buoyancy forcing (see also the sea level discussion in Chapter 6.1). Griffies & Greatbatch (2012) build on the work of Greatbatch (1994) by detailing how physical processes impact global mean sea level in ocean models.

#### 5.1.2.4. THERMO-HYDRODYNAMIC EQUATIONS FOR A FINITE REGION

Our next step in developing the equations of an ocean model involves integrating the continuum parcel equations over a finite region, with the region boundaries generally moving and permeable. The resulting budget equations form the basis for a finite volume discretization of the ocean equations. They may also be used to develop basin-wide budgets for purposes of large-scale analysis (Section 5.1.3.2). The finite volume approach serves our pedagogical aims, and it forms the basis for most ocean models in use today for large-scale studies. We make reference to the schematic shown in Figure 5.1.2 relevant for a numerical model.

##### Finite volume budget for scalars and momentum

Consider a volume of fluid,  $V$ , with a moving and permeable boundary  $S$ . The tracer mass budget within this region satisfies

$$\frac{\partial}{\partial t} \left( \int_V C \rho \, dV \right) = - \int_S \hat{\mathbf{n}} \cdot [(\mathbf{v} - \mathbf{v}^S) \rho C + \mathbf{J}] \, dS, \quad (5.1.18)$$

where we ignored tracer source/sink terms for brevity, dropped the superscript ( $C$ ) on the subgrid scale tracer flux  $\mathbf{J}$ , and wrote  $\hat{\mathbf{n}}$  for the outward normal to the boundary. Tracer mass within a region (left hand side) changes due to the passage of tracer through the boundary, either from advective transport or subgrid scale transport (right hand side). Advective transport is measured according to the normal projection of the fluid velocity in a frame moving with the surface,  $\mathbf{v} - \mathbf{v}^S$ . The subgrid scale tracer transport must likewise be measured relative to the moving surface. The finite volume budget for seawater mass is obtained by setting the tracer concentration to a constant in the tracer budget (5.1.18)

$$\frac{\partial}{\partial t} \left( \int_V \rho \, dV \right) = - \int_S \hat{\mathbf{n}} \cdot (\mathbf{v} - \mathbf{v}^S) \rho \, dS. \quad (5.1.19)$$

292 The relation between the mass budget (5.1.19) and tracer budget (5.1.18) is a manifes-  
 293 tation of the compatibility condition discussed following the continuum tracer equation  
 294 (5.1.7). An analogous finite volume budget follows for the hydrostatic primitive equa-  
 295 tions, in which we consider the horizontal momentum over a finite region with the  
 296 Coriolis Force in its simplified form (5.1.14)

$$\begin{aligned} \partial_t \left( \int_V \mathbf{u} \rho \, dV \right) = & - \int_V [g \hat{\mathbf{z}} + (f + \mathcal{M}) \hat{\mathbf{z}} \wedge \mathbf{u}] \rho \, dV \\ & - \int_S [\hat{\mathbf{n}} \cdot (\mathbf{v} - \mathbf{v}^S)] \mathbf{u} \rho \, dS + \int_S \hat{\mathbf{n}} \cdot (\boldsymbol{\tau} - \mathbf{I} p) \, dS. \end{aligned} \quad (5.1.20)$$

297 The volume integral on the right hand side arises from the gravitational and Corio-  
 298 lis body forces, whereas the surface integrals arise from both advective transport and  
 299 contact forces associated with stress and pressure.

300 Some domain boundaries are static, such as the lateral boundaries for a model grid  
 301 cell or the solid earth boundaries of an ocean basin (Figure 5.1.2). However, vertical  
 302 boundaries are quite often moving, with the ocean free surface

$$z = \eta(x, y, t) \quad (5.1.21)$$

303 a canonical example. In this case, the projection of the boundary velocity onto the  
 304 normal direction is directly proportional to the time tendency of the free surface

$$\hat{\mathbf{n}} \cdot \mathbf{v}^S = \left( \frac{\partial \eta}{\partial t} \right) |\nabla(z - \eta)|^{-1}. \quad (5.1.22)$$

305 Iso-surfaces of a generalized vertical coordinate

$$s = s(x, y, z, t) \quad (5.1.23)$$

306 are generally space and time dependent. For example, the grid cell top and bottom  
 307 may be bounded by surfaces of constant pressure, potential density, or another moving  
 308 surface. Here, the normal component of the surface velocity is proportional to the  
 309 tendency of the generalized vertical coordinate

$$\hat{\mathbf{n}} \cdot \mathbf{v}^S = - \left( \frac{\partial s}{\partial t} \right) |\nabla s|^{-1}. \quad (5.1.24)$$

### 310 Generalized vertical coordinates and dia-surface transport

311 To make use of a finite volume budget for layers defined by generalized vertical co-  
 312 ordinates requires that the vertical coordinate be monotonically stacked in the vertical,  
 313 so that there is a one-to-one relation between the geopotential coordinate,  $z$ , and the  
 314 generalized vertical coordinate. Mathematically, this constraint means that the *specific*  
 315 *thickness*  $\partial s / \partial z$  never vanishes, and thus remains of one sign throughout the domain  
 316 so there are no inversions in the generalized vertical coordinate iso-surfaces. An im-  
 317 portant case where  $\partial s / \partial z = 0$  occurs for isopycnal models in regions of zero vertical  
 318 density stratification. Handling such regions necessitates either a transformation to a  
 319 stably stratified vertical coordinate such as pressure, as in the Hybrid Ocean Model

320 (HYCOM) code of Bleck (2002), or appending a bulk mixed layer (Hallberg, 2003)  
 321 to the interior isopycnal layers as in the Miami Isopycnal Coordinate Ocean Model  
 322 (MICOM) code of Bleck (1998), or the General Ocean Layer Dynamics (GOLD) code  
 323 used in Adcroft et al. (2010).

The monotonic assumption (i.e.,  $\partial s/\partial z$  remains single signed) allows us to measure the advective transport across the constant  $s$  surfaces according to the dia-surface velocity component (Section 2.2 of Griffies & Adcroft (2008))

$$\rho w^{(s)} \equiv \frac{(\text{MASS/TIME}) \text{ OF FLUID THRU SURFACE}}{\text{AREA OF HORIZ PROJECTION OF SURFACE}} \quad (5.1.25a)$$

$$= \frac{\hat{\mathbf{n}} \cdot (\mathbf{v} - \mathbf{v}^S) \rho \, dS}{dA}, \quad (5.1.25b)$$

where  $dA$  is the horizontal projection of the surface area  $dS$ . Questions of how to measure dia-surface mass transport arise in many areas of ocean model formulation as well as construction of budgets for ocean domains. We present here two equivalent expressions

$$w^{(s)} = \left( \frac{\partial z}{\partial s} \right) \frac{ds}{dt} \quad (5.1.26a)$$

$$= w - (\partial_t + \mathbf{u} \cdot \nabla_s) z, \quad (5.1.26b)$$

in which  $\nabla_s z = -(\partial z/\partial s) \nabla_z s$  is the slope of the  $s$  surface as projected onto the horizontal plane (Chapter 6 of Griffies (2004)). Equation (5.1.26a) indicates that if the vertical coordinate has zero material time derivative, then there is zero dia-surface mass transport. Equation (5.1.26b) is commonly encountered when studying subduction of water from the mixed layer to the ocean interior, in which the generalized vertical coordinate is typically an isopycnal or isotherm (e.g., Marshall et al. (1999)). A final example of dia-surface transport arises from motion across the ocean free surface at  $z = \eta(x, y, t)$ , in which case

$$Q_m \, dA \equiv (\text{MASS/TIME}) \text{ OF FLUID THROUGH FREE SURFACE} \quad (5.1.27a)$$

$$= -dA (w - \mathbf{u} \cdot \nabla \eta - \partial_t \eta) \rho, \quad (5.1.27b)$$

324 with  $Q_m > 0$  if mass enters the ocean. Rearrangement leads to the surface kinematic  
 325 boundary condition

$$\rho (\partial_t + \mathbf{u} \cdot \nabla) \eta = w + Q_m \quad \text{at } z = \eta. \quad (5.1.28)$$

### 326 Surface and bottom boundary conditions

327 The tracer flux leaving the ocean through the free surface is given by (see equation  
 328 (5.1.18))

$$\int_{z=\eta} \hat{\mathbf{n}} \cdot [(\mathbf{v} - \mathbf{v}^S) \rho C + \mathbf{J}] \, dS = \int_{z=\eta} (-Q_m C + J^{(s)}) \, dA, \quad (5.1.29)$$

329 where

$$dA \, J^{(s)} = dS \, \hat{\mathbf{n}} \cdot \mathbf{J} \quad (5.1.30)$$

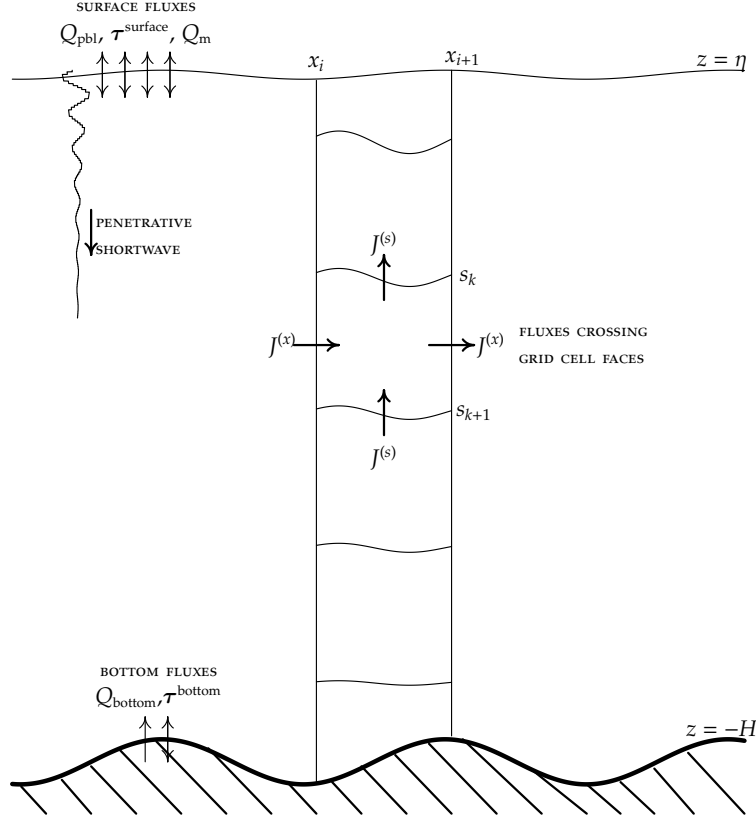


Figure 5.1.2: A longitudinal-vertical slice of ocean fluid from the surface at  $z = \eta(x, y, t)$  to bottom at  $z = -H(x, y)$ , along with a representative column of discrete grid cells (a latitudinal-vertical slice is analogous). Most ocean models used for large-scale climate studies assume the horizontal boundaries of a grid cell at  $x_i$  and  $x_{i+1}$  are static, whereas the vertical extent, defined by surfaces of constant generalized vertical coordinate  $s_k$  and  $s_{k+1}$ , can be time dependent. The tracer flux  $\mathbf{J}$  is decomposed into horizontal and dia-surface components, with the convergence of these fluxes onto a grid cell determining the evolution of tracer content within the cell. Similar decomposition occurs for momentum fluxes. Additional terms contributing to the evolution of tracer include source terms, and momentum evolution also includes body forces (Coriolis and gravity). Amongst the fluxes crossing the ocean surface, the shortwave flux penetrates into the ocean column as a function of the optical properties of seawater (e.g., Manizza et al., 2005).

330 is the dia-surface tracer transport associated with subgrid scale processes and/or param-  
 331 eterized turbulent boundary fluxes. Boundary fluxes are often given in terms of bulk  
 332 formula (see, e.g., Taylor (2000), Appendix C of Griffies et al. (2009), and Section  
 333 5.1.3.1), allowing for the boundary flux to be written in the form

$$-\int_{z=\eta} \hat{\mathbf{n}} \cdot [(\mathbf{v} - \mathbf{v}^S) \rho C + \mathbf{J}] dS = \int_{z=\eta} (Q_m C_m + Q_{pbl}) dA, \quad (5.1.31)$$

where  $C_m$  is the tracer concentration within the incoming mass flux  $Q_m$ . The first term on the right hand side of equation (5.1.31) represents the advective transport of tracer through the surface with the water (i.e., ice melt, rivers, precipitation, evaporation). The term  $Q_{\text{pbl}}$  arises from parameterized turbulence and/or radiative fluxes within the surface planetary boundary layer, such as sensible, latent, shortwave, and longwave heating as occurs for the temperature equation, with  $Q_{\text{pbl}} > 0$  signaling tracer entering the ocean through its surface. A similar expression to (5.1.31) holds at the ocean bottom  $z = -H(x, y)$ , though it is common in climate modeling to only consider geothermal heating (Adcroft et al., 2001; Emile-Geay & Madec, 2009) with zero mass flux.

The force acting on the bottom surface of the ocean is given by

$$\mathbf{F}_{\text{bottom}} = - \int_{z=-H} [\nabla(z+H) \cdot \boldsymbol{\tau} - p \nabla(z+H)] dA. \quad (5.1.32)$$

In the presence of a nonzero topography gradient,  $\nabla H \neq 0$ , the term  $-p \nabla H$  at the ocean bottom gives rise to a topographic *form stress* that affects horizontal momentum. Such stress is especially important for strong flows that reach to the ocean bottom, such as in the Southern Ocean (Chapter 4.8). Parameterization of this stress is particularly important for models that only resolve a coarse-grained representation of topography. In addition to form stress, we assume that a boundary layer model, typically in the form of a drag law, provides information so that we can parameterize the bottom vector stress

$$\boldsymbol{\tau}^{\text{bottom}} \equiv \nabla(z+H) \cdot \boldsymbol{\tau} \quad \text{at } z = -H \quad (5.1.33)$$

associated with bottom boundary layer momentum exchange. This parameterization of bottom stress necessarily incorporates interactions between the ocean fluid with small scale topography variations, so that there is a non-zero vector stress  $\boldsymbol{\tau}^{\text{bottom}}$  even if the large-scale topography resolved by a numerical model is flat. Additional considerations for the interactions between unresolved mesoscale eddies with topography lead to the Neptune parameterization of Holloway (1986, 1989, 1992).

Momentum transfer through the ocean surface is given by

$$\mathbf{F}_{\text{surface}} = \int_{z=\eta} [\boldsymbol{\tau}^{\text{surface}} - p_a \nabla(z-\eta) + Q_m \mathbf{u}_m] dA. \quad (5.1.34)$$

In this equation,  $\mathbf{u}_m$  is the horizontal velocity of the mass transferred across the ocean boundary. This velocity is typically taken equal to the velocity of the ocean currents in the top cell of the ocean model, but such is not necessarily the case when considering the different velocities of, say, river water and precipitation. The vector stress

$$\boldsymbol{\tau}^{\text{surface}} \equiv \nabla(z-\eta) \cdot \boldsymbol{\tau} \quad \text{at } z = \eta \quad (5.1.35)$$

arises from the wind, as well as interactions between the ocean and ice. As for the bottom stress parameterization (5.1.33), a boundary layer model determining the surface vector stress,  $\boldsymbol{\tau}^{\text{surface}}$ , must consider subgrid-scale fluctuations of the sea surface, such as nonlinear effects associated with surface waves (Sullivan & McWilliams, 2010; Cavalieri et al., 2012; Belcher et al., 2012). Finally, we take the applied pressure at  $z = \eta$  to

368 equal the pressure  $p_a$  from the media sitting above the ocean; namely, the atmosphere  
 369 and ice. As for the bottom force, there is generally a nonzero horizontal projection of  
 370 the applied pressure acting on the curved free surface,  $p_a \nabla \eta$ , thus contributing to an  
 371 applied surface pressure form stress on the ocean.

#### 372 5.1.2.5. PHYSICAL CONSIDERATIONS FOR TRANSPORT

373 Working with a discrete rather than continuous fluid presents many fundamental  
 374 and practical issues. One involves the introduction of unphysical *computational modes*  
 375 whose presence can corrupt the simulation; e.g., dispersion arising from discrete advec-  
 376 tion operators can lead to spurious mixing (Griffies et al. (2000b), Ilicak et al. (2012)).  
 377 Another issue involves the finite grid size,  $\Delta$ , or more generally the finite degrees of  
 378 freedom available to simulate a continuum fluid. The grid scale is generally many  
 379 orders larger than the Kolmogorov scale (equation (5.1.1))

$$\Delta \gg L_{\text{Kol}}, \quad (5.1.36)$$

380 and  $\Delta$  determines the degree to which an oceanic flow feature can be resolved by a  
 381 simulation.

382 There are two reasons to parameterize a physical process impacting the ocean. The  
 383 first is if the process is filtered from the continuum equations forming the basis for  
 384 the model, such as the hydrostatic approximation (5.1.16). The second concerns the  
 385 finite grid scale. To understand how the grid introduces a closure or parameterization  
 386 problem, consider a *Reynolds decomposition* of an advective flux

$$\overline{u\psi} = \overline{u}\overline{\psi} + \overline{u'\psi'}, \quad (5.1.37)$$

387 where  $u = \overline{u} + u'$  expresses a velocity component as the sum of a mean and fluctu-  
 388 ation, and the average of a fluctuating field is assumed to vanish,  $\overline{u'} = 0$ . The same  
 389 decomposition is assumed for the field being transported,  $\psi$ , which could be a tracer  
 390 concentration or velocity component. The discrete grid represents the product of the  
 391 averaged fields,  $\overline{u}\overline{\psi}$ , through a numerical advection operator. Computing this resolved  
 392 transport using numerical methods is the *representation problem*, which involves spec-  
 393 ification of a numerical advection operator. The correlation term,  $\overline{u'\psi'}$ , is not explicitly  
 394 represented on the grid, with its specification constituting the *subgrid scale parame-*  
 395 *terization problem*. The correlation term is referred to as a *Reynolds stress* if  $\psi$  is a  
 396 velocity component, and an *eddy flux* if  $\psi$  is a tracer. To deduce information about  
 397 the second order correlation  $\overline{u'\psi'}$  requires third order correlations, which are functions  
 398 of fourth order correlations, etc., thus forming the *turbulence closure problem*. Each  
 399 process depicted in Figure 5.1.1 contributes to fluctuations, so they each engender a  
 400 closure problem if unresolved.

401 The theory required to produce *mean field* or averaged fluid equations is extensive  
 402 and nontrivial. A common aim is to render the resulting subgrid scale correlations  
 403 in a form subject to physical insight and sensible parameterization. The variety of  
 404 averaging methods amount to different mathematical approaches that are appropriate  
 405 under differing physical regimes and are functions of the vertical coordinates used to  
 406 describe the fluid. A non-exhaustive list of examples specific to the ocean include the  
 407 following (see also Olbers et al. (2012) for further discussion of even more averaging  
 408 methods).

- 409 • The microscale or infra-grid averaging of DeSzoeke & Bennett (1993), Davis  
410 (1994a), Davis (1994b), and DeSzoeke (2009) focuses on scales smaller than a  
411 few tens of metres.
- 412 • The density weighted averaging of Hesselberg (1926) (see also McDougall et al.  
413 (2002) and Chapter 8 of Griffies (2004)), provides a framework to account for  
414 the mass conserving character of the non-Boussinesq ocean equations, either  
415 hydrostatic or non-hydrostatic.
- 416 • The isopycnal thickness weighted methods of DeSzoeke & Bennett (1993), Mc-  
417 Dougall & McIntosh (2001), DeSzoeke (2009), and Young (2012) (see also  
418 Chapter 9 of Griffies (2004)) provide a framework to develop parameterizations  
419 of mesoscale eddy motions in the stratified ocean interior; see also the combined  
420 density and thickness weighted methods of Greatbatch & McDougall (2003).  
421 Eden et al. (2007) propose an alternative that averages over the same mesoscale  
422 phenomena, but maintains an Eulerian perspective rather than moving to isopy-  
423 cnal space.

424 There are few robust, and even fewer first principle, approaches to parameteriza-  
425 tion, with simulations often quite sensitive to the theoretical formulation as well as  
426 specific details of the numerical implementation. One may choose to ignore the topic  
427 of parameterizations, invoking an *implicit large eddy simulation* (ILES) philosophy  
428 (Margolin et al. (2006), Grinstein et al. (2007), Shchepetkin & McWilliams (1998)),  
429 whereby the responsibility for closing the transport terms rests on the numerical meth-  
430 ods used to represent advection. For large-scale modeling, especially with applications  
431 to climate, this approach is not common since the models are far from resolving many  
432 of the known important dynamical scales, such as the mesoscale. However, it is useful  
433 to test this approach to expose simulation features where the absence of a parameter-  
434 ization leads to obvious biases. Delworth et al. (2012) provides one such example, in  
435 which the ocean model component of a coupled climate model permits, but does not re-  
436 solve, mesoscale eddies, and yet there is no parameterization of the unresolved portion  
437 of the mesoscale eddies. Determining methods of mesoscale parameterization for use  
438 in mesoscale eddy permitting models is an active research area. In general, simulations  
439 extending over decadal to longer times must confront an ocean whose circulation and  
440 associated water masses are fundamentally impacted by the zoo of physical processes  
441 depicted in Figure 5.1.1, most of which are unresolved and have nontrivial impacts on  
442 the simulation.

### 443 **Parameterizing transport in a stratified ocean**

444 In an ideal ocean without mixing, tracer concentration is reversibly stirred by the re-  
445 solved velocity field (Eckart, 1948). That is, tracer concentration is materially constant  
446 (equation (5.1.5) with zero right hand side), and all tracer iso-surfaces are impenetra-  
447 ble to the resolved fluid flow. Mixing changes this picture, with molecular diffusion  
448 the ultimate cause of mixing and irreversibility. Upon averaging the equations accord-  
449 ing to the grid scale of a numerical model of a stratified ocean, subgrid eddy tracer  
450 fluxes associated with mesoscale eddies are generally parameterized by downgradient  
451 diffusion oriented according to neutral directions (Solomon, 1971; Redi, 1982), with

452 this parameterization termed *neutral*, *epineutral*, or *isoneutral* diffusion. As noted by  
 453 Gent & McWilliams (1990), there is an additional eddy advective flux (see also Gent  
 454 et al. (1995) and Griffies (1998)). Over the past decade, the use of such *neutral physics*  
 455 parameterizations has become ubiquitous in ocean climate models since they generally  
 456 improve simulations of water masses (Chapter 3.4).

457 *Dianeutral* processes mix material across neutral directions (Chapter 3.3). These  
 458 processes arise from enhanced mixing in upper and lower boundary layers (e.g., Large  
 459 et al. (1994), Legg et al. (2009)), as well as regions above rough topography (Polzin  
 460 et al. (1997), Toole et al. (1997), Kunze & Sanford (1996), Naveira-Garabato et al.  
 461 (2004), Kunze et al. (2006), MacKinnon et al. (2010)). Dianeutral mixing in the ocean  
 462 interior away from rough topography is far smaller (Ledwell et al., 1993, 2011). Ad-  
 463 ditionally, double diffusive processes (salt fingering and diffusive convection) arise  
 464 from the differing rates for heat and salt diffusion (Schmitt, 1994). Finally, cabbel-  
 465 ing and thermobaricity (Chapter 3.2) may play an important role in dianeutral transport  
 466 within the ocean interior, especially in the Southern Ocean (Marsh (2000), Iudicone  
 467 et al. (2008), Klocker & McDougall (2010)). Cabbeling and thermobaricity arise from  
 468 epineutral mixing of temperature and salinity in the presence of the nonlinear equation  
 469 of state for seawater (McDougall (1987)).

470 Although vigorous in parts of the ocean, dianeutral transport is extremely small in  
 471 other parts in comparison to the far larger epineutral transport. Indeed, ocean mea-  
 472 surements indicate that the ratio of dianeutral to epineutral transport is roughly  $10^{-8}$  in  
 473 many regions away from boundaries and above relatively smooth bottom topography  
 474 (Ledwell et al., 1993, 2011), and it can become even smaller at the equator (Gregg  
 475 et al., 2003). Although tiny by comparison for much of the ocean, dianeutral transport  
 476 in the ocean interior is in fact an important process involved with modifying vertical  
 477 stratification. Consequently, it impacts fundamentally on the ocean’s role in climate. In  
 478 ocean climate models, the parameterization of interior dianeutral mixing has evolved  
 479 from a prescribed and static vertical diffusivity proposed by Bryan & Lewis (1979), to  
 480 a collection of subgrid scale processes largely associated with breaking internal gravity  
 481 waves and other sources of enhanced vertical shear (e.g., Large et al. (1994), Simmons  
 482 et al. (2004), Jackson et al. (2008), Melet et al. (2013)) (Chapter 3.2).

### 483 **Two emerging ideas for parameterization**

484 We mention two emerging approaches to account for subgrid scale processes that  
 485 may impact on ocean climate modeling in the near future. Although much work re-  
 486 mains to determine whether either will become practical, there are compelling physical  
 487 and numerical reasons to give these proposals serious investigation.

488 **STOCHASTIC CLOSURE.** Hasselmann (1976) noted that certain components of the climate  
 489 system can be considered a stochastic, or noise, forcing that contributes to the vari-  
 490 ability of other components. The canonical example is an ocean that transfers the  
 491 largely white noise fluctuations from the atmospheric weather patterns into a red noise  
 492 response (i.e., increased power at the low frequencies) (Frankignoul & Hasselmann  
 493 (1977), Hall & Manabe (1997)). More recently, elements of the atmospheric and cli-  
 494 mate communities have considered a stochastic term in the numerical model equations  
 495 used for weather forecasting and climate projections, with particular emphasis on the



496 utility for tropical convection; e.g., see Williams (2005) and Palmer & Williams (2008)  
 497 for pedagogical discussions. This noise term is meant to parameterize elements of  
 498 unresolved fluctuations as they feedback onto the resolved fields.

499 Depending on the phenomena, there are cases where subgrid scale ocean fields  
 500 are indeed fluctuating chaotically. Furthermore, the averaging operation applied to the  
 501 nonlinear terms does not generally satisfy the Reynolds assumption of zero average for  
 502 the fluctuating terms (i.e.,  $\overline{u' \neq 0}$ ) (Davis (1994b), DeSzoeke (2009)). So along with the  
 503 compelling results from atmospheric models, there are reasons to consider introducing  
 504 a stochastic element to the subgrid scale terms used in an ocean model (Berlov, 2005;  
 505 Brankart, 2013; Kitsios et al., 2013).

506 **SUPER-PARAMETERIZATION.** In an effort to improve the impact of atmospheric convec-  
 507 tive processes on the large-scale, Grabowski (2001) embedded a two-dimensional non-  
 508 hydrostatic model into a three-dimensional large-scale hydrostatic primitive equation  
 509 model. The non-hydrostatic model feeds information to the hydrostatic model about  
 510 convective processes, and the hydrostatic model in turn provides information about the  
 511 large-scale to the non-hydrostatic model. Khairoutdinov et al. (2008) further examined  
 512 this *super-parameterization* approach and showed some promising results. Campin  
 513 et al. (2011) in turn have applied the approach to oceanic convection (see Figure  
 514 5.1.3). Some processes are perhaps not parameterizable, and so must be explicitly  
 515 represented. Additionally, some processes are not represented or parameterized well  
 516 using a particular modeling framework. Both of these cases may lend themselves to  
 517 super-parameterizations.

518 We consider a super-parameterization to be the use of a sub-model (or child model)  
 519 that is two-way embedded into the main or parent-model, with the sub-model focused  
 520 on representing certain processes that the parent-model either cannot resolve or does  
 521 a poor job of representing due to limitations of its numerical methods. In this regard,  
 522 super-parameterization ideas share features with two-way nesting approaches (Debreu  
 523 & Blayo, 2008), in which a nested fine grid region resolves processes that the coarse  
 524 grid parent-model cannot (we have more to say on nesting in Section 5.1.3.1). The ap-  
 525 proach of Bates et al. (2012a,b) is another example, in which a dynamic and interactive  
 526 three-dimensional Lagrangian sub-model is embedded in an Eulerian model.

### 527 **Where we stand with physical parameterizations**

528 Many of the same questions regarding parameterizations raised in the review of  
 529 Griffies et al. (2000a) remain topical in the research community today. This longevity  
 530 is both a reflection of the difficulty of the associated theoretical and numerical issues,  
 531 and the importance of developing robust parameterizations suitable for a growing suite  
 532 of applications. We offer the following assessment regarding the parameterization  
 533 question:

534 A NECESSARY CONDITION FOR THE EVALUATION OF A PHYSICAL PROCESS PARAM-  
 535 ETERIZATION IN GLOBAL OCEAN CLIMATE SIMULATIONS IS TO EXAMINE COMPANION  
 536 CLIMATE SIMULATIONS THAT FULLY RESOLVE THE PROCESS.

537 That is, we will not know the physical integrity of a parameterization until the param-  
 538 eterized process is fully resolved. This assessment does not mean that comparisons

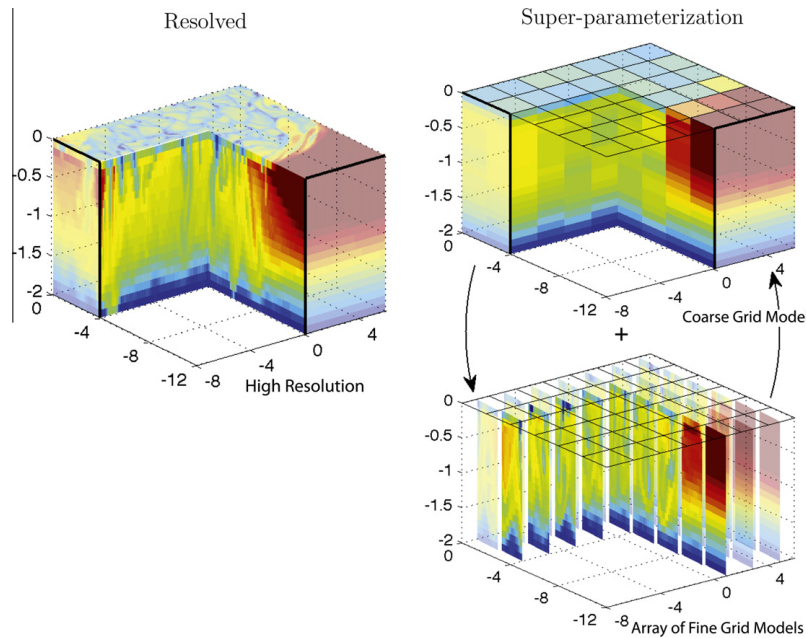


Figure 5.1.3: Three-dimensional view of the temperature field (red is warm, blue is cold) in two simulations of chimney convection similar to Jones & Marshall (1993). Left side: from a high resolution simulation which resolves small scale plume processes. Right side: from a super-parameterized model in which a coarse-grain (CG) large-scale model (top right panel) representing balanced motion is integrated forward with embedded fine-grained (FG) (bottom right panel) running at each column of the large-scale grid. The FG is non-hydrostatic and attempts to resolve the small-scale processes. The FGs and the CG are integrated forward together and exchange information following the algorithm set out in Campin et al. (2011). This figure is based on Figure 1 of Campin et al. (2011).

539 between models and field observations, laboratory studies, or process studies, are irrelevant to the parameterization question. It does, however, summarize the situation with  
 540 regard to certain phenomena such as the mesoscale, as supported with recent experience  
 541 studying the Southern Ocean response to wind stress changes. As shown by Farneti  
 542 et al. (2010), mesoscale eddy models respond in a manner closer to the observational  
 543 analysis from Böning et al. (2008) than certain coarse resolution non-eddy models  
 544 using parameterizations. Prompted by this study, numerous authors have made compelling  
 545 suggestions for improving the mesoscale eddy parameterizations (e.g., Farneti  
 546 & Gent (2011), Hofmann & Morales-Maqueda (2011), Gent & Danabasoglu (2011)).  
 547

548 The above assessment does not undermine the ongoing quest to understand processes,  
 549 such as mesoscale eddy transport, and to develop parameterizations for use in  
 550 coarse grid models. However, it does lend a degree of humility to those arguing for  
 551 the validity of their favorite parameterization. It also supports the use of ensembles  
 552 of model simulations whose members differ by perturbing the physical parameteriza-  
 553 tions and numerical methods in sensible manners to more fully test the large space of

554 unknown parameters.

#### 555 5.1.2.6. NUMERICAL CONSIDERATIONS FOR TRANSPORT

556 We propose the following as an operational definition for resolution of a flow fea-  
557 ture.

558 A FLOW FEATURE IS *resolved* ONLY SO FAR AS THERE ARE NO LESS THAN  $2\pi$  GRID  
559 POINTS SPANNING THE FEATURE.

560 This definition is based on resolving a linear wave with a discrete, non-spectral, repre-  
561 sentation so that any admitted wave has length no smaller than  $2\pi\Delta$ . We consider this a  
562 sensible operational definition even when representing nonlinear and turbulent motion.  
563 Decomposing the flow into vertical baroclinic modes, one is then led to considering the  
564 baroclinic flow as resolved only so far as there are  $2\pi$  grid points for each baroclinic  
565 wave whose contribution to the flow energy is nontrivial. Traditionally we write the  
566 Rossby radius as  $R = 1/\kappa$ , with the wavenumber  $\kappa = 2\pi/\lambda$  and  $\lambda$  the baroclinic wave-  
567 length. Hence, if the grid spacing is less than the Rossby radius,  $\Delta \leq R$ , then the grid  
568 indeed resolves the corresponding baroclinic wave since  $2\pi\Delta \leq \lambda$ . As the first baro-  
569 clinic mode dominates much of the mid-latitude ocean (Wunsch & Stammer (1995),  
570 Wunsch (1997), Stammer (1998), Smith & Vallis (2001), Smith (2007)), modelers gen-  
571 erally look to the first baroclinic Rossby radius as setting the scale whereby baroclinic  
572 flow is resolved (Smith et al. (2000)). Higher baroclinic modes, submesoscale modes  
573 (Boccaletti et al. (2007), Fox-Kemper et al. (2008), Klein & Lapeyre (2009)), internal  
574 gravity wave modes (Arbic et al., 2010), and other filamentary features require even  
575 finer resolution.

#### 576 Ensuring that admitted flow features are resolved

577 Nonlinear eddying flows contain waves with many characteristic lengths, and tur-  
578 bulent flows experience an energy and variance cascade between scales (see Section  
579 5.1.2.2 or Vallis (2006)). Furthermore, in the presence of a strongly nonlinear flow,  
580 certain discretizations of the nonlinear self-advection term  $\rho \mathbf{v} \cdot \nabla \mathbf{v}$  (see equation (5.1.12))  
581 can introduce grid scale energy even when the eddying flow is geostrophic and thus  
582 subject to the inverse cascade. So quite generally, resolving all flow features admitted  
583 in a simulation requires one to minimize the energy and variance contained at scales  
584 smaller than  $2\pi\Delta$ .

585 There are two general means to dissipate energy and variance of unresolved flow  
586 features. The implicit LES approach places responsibility for dissipation with the  
587 numerical advection operators acting on momentum and tracer. When coupled to a  
588 highly accurate underlying discretization of the advection fluxes, and with a mono-  
589 tonicity constraint that retains physically sensible values for the transport field, such  
590 numerical transport operators can be constructed to ensure that only well resolved flow  
591 features are admitted. The Regional Ocean Model System (ROMS) (Shchepetkin &  
592 McWilliams, 2005) has incorporated elements of this approach, in which lateral fric-  
593 tion or diffusion operators are not required for numerical purposes.

594 The second approach to dissipating unresolved flow features is to incorporate a  
595 friction operator into the momentum equation, and diffusion operator into the tracer

equation, each using a transport coefficient that is far larger than molecular. There are straightforward ways to do so, yet a naive use of these methods can lead to over-dissipation of the simulation (Griffies & Hallberg (2000), Large et al. (2001), Smith & McWilliams (2003), Jochum (2009)), and/or spurious dianeutral mixing associated with diffusion across density fronts (Veronis (1975), Roberts & Marshall (1998)). Consequently, more sophisticated dissipation operators are typically considered, with their design based on a mix between physical and numerical needs (e.g., see Chapter 14 of Griffies (2004)).

### Representing transport in a numerical ocean

The extreme anisotropy between dianeutral and epineutral transport in the ocean interior has motivated the development of ocean models based on potential density as the vertical coordinate (see Section 5.1.2.7). Respecting the epineutral/dianeutral anisotropy in non-isopycnal models is a nontrivial problem in three-dimensional numerical transport. Level models or terrain following models must achieve small levels of spurious dianeutral mixing through a combination of highly accurate tracer advection schemes, and properly chosen momentum and tracer closure schemes, all in the presence of hundreds to thousands of mesoscale eddy turnover times and a nonlinear equation of state.

As noted by Griffies et al. (2000a), resolving all flow features (see Section 5.1.2.6) is difficult for mesoscale eddy simulations, since eddies pump tracer variance to the grid scale and thus increase tracer gradients. At some point, a tracer advection scheme will either produce dispersive errors, and so introduce spurious extrema and thus expose the simulation to spurious convection, or add dissipation via a mixing operator or low order upwind biased advection operator in order to preserve monotonicity.

### Methods for reducing spurious dianeutral transport

Mechanical energy cascades to the large scale in a geostrophically turbulent flow. However, grid scale energy can appear as the nonlinear advection of momentum becomes more dominant with eddies, thus stressing the numerical methods used to transport momentum. This issue is directly connected to the spurious dianeutral tracer transport problem, since even very accurate tracer advection schemes, such as the increasingly popular scheme from Prather (1986) (see Maqueda & Holloway (2006), Tatebe & Hasumi (2010), Hill et al. (2012) for ocean model examples) will be exposed to unphysically large spurious transport and/or dispersion error (which produce tracer extrema) if the velocity field contains too much energy (i.e., noise) near the grid scale. Hence, the integrity of momentum transport, and the associated momentum closure, becomes critical for maintaining physically sensible tracer transport, particularly with an eddy flow or any flow where momentum advection is important (Ilicak et al., 2012).

Results from Griffies et al. (2000a), Jochum et al. (2008), and Ilicak et al. (2012) emphasize the need to balance the quest for more kinetic energy, which generally pushes the model closer to observed energy levels seen in satellites (see, e.g., Figure 5.1.4 discussed in Section 5.1.3, or Chapter 2.2), with the need to retain a negligible spurious potential energy source whose impact accumulates over decades and longer.

639 Following Ilicak et al. (2012), we suggest that maintaining a grid Reynolds number so  
640 that

$$\text{Re}_\Delta = \frac{U \Delta}{\nu} < 2 \quad (5.1.38)$$

641 ensures unresolved flow features are adequately filtered. In this equation,  $U$  is the  
642 velocity scale of currents admitted in the simulation,  $\Delta$  is the grid scale, and  $\nu$  is the  
643 generally non-constant Laplacian eddy viscosity used to dissipate mechanical energy.

644 The constraint (5.1.38) has multiple origins. One is associated with the balance be-  
645 tween advection and diffusion in a second order discretization (see Bryan et al. (1975)  
646 or Section 18.1.1 of Griffies (2004)), in which  $\text{Re}_\Delta < 2$  eliminates an unphysical mode.  
647 More recently, Ilicak et al. (2012) identified this constraint as necessary to ensure that  
648 spurious diapycnal mixing is minimized. ROMS (Shchepetkin & McWilliams, 2005)  
649 has this constraint built into the advection of momentum, whereas most other codes  
650 require specification of a friction operator. Selective use of a flow dependent viscos-  
651 ity, such as from a Laplacian or biharmonic Smagorinsky scheme (see Smagorinsky  
652 (1993), Griffies & Hallberg (2000), or Section 18.3 of Griffies (2004)), or the scheme  
653 of Leith (1996) discussed by Fox-Kemper & Menemenlis (2008), assists in maintain-  
654 ing the constraint (5.1.38) while aiming to avoid over-dissipating kinetic energy in the  
655 larger scales.

#### 656 5.1.2.7. VERTICAL COORDINATES

657 There are three traditional approaches to choosing vertical coordinates: geopoten-  
658 tial, terrain-following, and potential density (isopycnal). Work continues within each  
659 model class to expand its regimes of applicability, with significant progress occurring  
660 in many important areas. The review by Griffies et al. (2010) provides an assessment  
661 of recent efforts, which we now summarize.

662 We start this discussion by noting that all vertical coordinates found to be useful  
663 in ocean modeling remain “vertical” in the sense they retain a simple expression for  
664 the hydrostatic balance (5.1.16), thus allowing for a hydrostatic balance to be triv-  
665 ially maintained in a simulation. This constraint is a central reason ocean and atmo-  
666 spheric modelers favour the projected non-orthogonal coordinates first introduced by  
667 Starr (1945), rather than locally orthogonal coordinates whose form of hydrostatic bal-  
668 ance is generally far more complex.

#### 669 Geopotential and generalized level models

670 Geopotential z-coordinate models have found wide-spread use in global climate  
671 applications for several reasons, such as their simplicity and straightforward nature  
672 of parameterizing the surface boundary layer and associated air-sea interaction. For  
673 example, of the 25 coupled climate models contributing to the CMIP3 archive used  
674 for the IPCC AR4 (Meehl et al., 2007), 22 employ geopotential ocean models, one is  
675 terrain-following, one is isopycnal, and one is hybrid pressure-isopycnal-terrain.

676 There are two key shortcomings ascribed to z-coordinate ocean models.

- 677 • **SPURIOUS MIXING:** This issue was discussed in Section 5.1.2.6.

- **OVERFLOWS:** Downslope flows (Legg, 2012) in z-models tend to possess excessive entrainment (Roberts & Wood (1997), Winton et al. (1998) Legg et al. (2006), Legg et al. (2008), Treguier et al. (2012)), and this behaviour compromises simulations of deep watermasses derived from dense overflows. Despite much effort and progress in understanding both the physics and numerics (Dietrich et al. (1987), Beckmann & Döschner (1997), Beckmann (1998), Price & Yang (1998), Killworth & Edwards (1999), Campin & Goosse (1999), Nakano & Sugimotohara (2002), Wu et al. (2007), Danabasoglu et al. (2010), Laanaia et al. (2010)), the representation/parameterization of overflows remains difficult at horizontal grid spacing coarser than a few kilometers (Legg et al., 2006).

A shortcoming related to the traditional representation of topography (e.g., Cox (1984)) has largely been overcome by partial cells now commonly used in level models (Adcroft et al. (1997), Pacanowski & Gnanadesikan (1998), Barnier et al. (2006)). It is further reduced by the use of a momentum advection scheme conserving both energy and enstrophy, and by reducing near-bottom sidewall friction (Penduff et al. (2007) and Le Sommer et al. (2009)). A complementary problem arises from the use of free surface geopotential coordinate models, whereby they can lose their surface grid cell in the presence of refined vertical spacing. Generalizations of geopotential coordinates, such as the stretched geopotential coordinate,  $z^*$ , introduced by Stacey et al. (1995) and Adcroft & Campin (2004), overcome this problem (see Griffies et al. (2011) and Dunne et al. (2012) for recent global model applications). Leclair & Madec (2011) introduce an extension to  $z^*$  that aims to reduce spurious diapycnal mixing. Additional efforts toward mass conserving non-Boussinesq models have been proposed by Huang et al. (2001), DeSzoek & Samelson (2002) and Marshall et al. (2004), with one motivation being the direct simulation of the global steric effect required for sea level studies (Greatbatch (1994), Griffies & Greatbatch (2012)). What has emerged from the geopotential model community is a movement towards such *generalized level* coordinates that provide enhanced functionality while maintaining essentially the physical parameterizations developed for geopotential models. We thus hypothesize that the decades of experience and continued improvements with numerical methods, parameterizations, and applications suggest that generalized level methods will remain in use for ocean climate studies during the next decade and likely much longer.

### Isopycnal layered and hybrid models

Isopycnal models generally perform well in the ocean interior, where flow is dominated by quasi-adiabatic dynamics, as well as in the representation/parameterization of dense overflows (Legg et al., 2006). Their key liability is that resolution is limited in weakly stratified water columns. For ocean climate simulations, isopycnal models attach a non-isopycnal surface layer to describe the surface boundary layer. Progress has been made with such *bulk mixed layer* schemes, so that Ekman driven restratification and diurnal cycling are now well simulated (Hallberg, 2003). Additionally, when parameterizing lateral mixing along constant potential density surfaces rather than neutral directions, isopycnal the models fail to incorporate diapycnal mixing associated with thermobaricity (McDougall, 1987) (see Section A.27 of IOC et al. (2010)). Iudicone et al. (2008) and Klocker & McDougall (2010) suggest that thermobaricity contributes

722 more to water mass transformation in the Southern Ocean than from breaking internal  
723 gravity waves.

724 Hybrid models offer an alternative means to eliminate liabilities of the various tra-  
725 ditional vertical coordinate classes. The HYCOM code of Bleck (2002) exploits ele-  
726 ments of the hybrid approach, making use of the Arbitrary Lagrangian-Eulerian (ALE)  
727 method for vertical remapping (Donea et al., 2004). As noted by Griffies et al. (2010),  
728 progress is being made to address issues related to the use of isopycnal layered models,  
729 or their hybrid brethren, thus providing a venue for the use of such models for a variety  
730 of applications, including global climate (Megann et al. (2010), Dunne et al. (2012)).

731 A physical system of growing importance for sea level and climate studies concerns  
732 the coupling of ocean circulation to ice shelves whose grounding lines can evolve. Re-  
733 quired of such models is a land-ocean boundary that evolves, in which case ocean  
734 models require a wetting and drying method. We have in mind the growing impor-  
735 tance of studies of coupled ice-shelf ocean processes with evolving grounding lines  
736 (Goldberg et al., 2012) (see Chapter 4.6 in this volume). Though not uncommon for  
737 coastal modeling applications, wetting and drying for ocean climate model codes re-  
738 main rare, with the study of Goldberg et al. (2012) using the GOLD isopycnal code of  
739 Adcroft et al. (2010) the first to our knowledge. It is notable that climate applications  
740 require exact conservation of mass and tracer to remain viable for long-term (decadal  
741 and longer) simulations, whereas certain of the wetting and drying methods used for  
742 coastal applications fail to meet this constraint. We conjecture that isopycnal mod-  
743 els, or their generalizations using ALE methods, will be very useful for handling the  
744 evolving coastlines required for such studies.

#### 745 **Terrain following vertical coordinate models**

746 Terrain-following coordinate models (TFCM) have found extensive use for coastal  
747 and regional applications, where bottom boundary layers and topography are well-  
748 resolved. As with geopotential models, TFCMs generally suffer from spurious dianeu-  
749 tral mixing due to problems with numerical advection (Marchesiello et al., 2009). Also,  
750 the formulation of neutral diffusion (Redi, 1982) and eddy-induced advection (Gent &  
751 McWilliams, 1990) has until recently not been considered for TFCMs. However, re-  
752 cent studies by Lemarié et al. (2012a,b) have proposed new methods to address both of  
753 these issues.

754 A well known problem with TFCMs is calculation of the horizontal pressure gradi-  
755 ent, with errors leading to potentially nontrivial spurious flows. Errors are a function of  
756 topographic slope and near-bottom stratification (Haney (1991), Deleersnijder & Beck-  
757 ers (1992), Beckmann & Haidvogel (1993), Mellor et al. (1998), and Shchepetkin &  
758 McWilliams (2002)). The pressure gradient problem has typically meant that TFCMs  
759 are not useful for global-scale climate studies with realistic topography, at least until  
760 horizontal grid spacing is very fine (order 10 km or finer). However, Lemarié et al.  
761 (2012b), following from Mellor et al. (1998), identify an intriguing connection be-  
762 tween pressure gradient errors and the treatment of lateral diffusive transport. Namely,  
763 the use of neutral diffusion rather than terrain-following diffusion in grids of order  
764 50 km with the Regional Ocean Model System (ROMS) (Shchepetkin & McWilliams,  
765 2005) significantly reduces the sensitivity of the simulation to the level of topographic

MODEL	VERTICAL COORDINATE	WEB SITE
HYCOM	hybrid $\sigma - \rho - p$	<a href="http://hycom.org/ocean-prediction">hycom.org/ocean-prediction</a>
MIT	general level	<a href="http://mitgcm.org/">mitgcm.org/</a>
MOM	general level	<a href="http://mom-ocean.org">mom-ocean.org</a>
NEMO	general level	<a href="http://nemo-ocean.eu/">nemo-ocean.eu/</a>
POM	terrain following	<a href="http://aos.princeton.edu/WWWPUBLIC/PROFS/NewPOMPage.html">aos.princeton.edu/WWWPUBLIC/PROFS/NewPOMPage.html</a>
POP	geopotential	<a href="http://climate.lanl.gov/Models/POP/">climate.lanl.gov/Models/POP/</a>
ROMS	terrain following	<a href="http://myroms.org/">myroms.org/</a>

Table 5.1.1: Open source ocean model codes with structured horizontal grids applicable for a variety of studies including large-scale circulation. These codes are currently undergoing active development (i.e., updated algorithms, parameterizations, diagnostics, applications), possess thorough documentation, and maintain widespread community support and use. Listed are the model names, vertical coordinate features, and web site where code and documentation are available. We failed to find other model codes that satisfy these criteria.

Each model is coded in Fortran with generalized orthogonal horizontal coordinates. MOM and POP use an Arakawa B-grid layout of the discrete momentum equations, whereas others use an Arakawa C-grid (see Griffies et al. (2000a) for a summary of B and C grids). General level models are based on the traditional  $z$ -coordinate approach, but may be generalized to include other vertical coordinates such as pressure or terrain following. HYCOM’s vertical coordinate algorithm is based on vertical remapping to return coordinate surfaces at each time step to their pre-defined targets. In contrast, general level models diagnose the dia-surface velocity component through the continuity equation (Adcroft & Hallberg, 2006), which is the fundamental distinction from general layered or quasi-Lagrangian models such as HYCOM.

Acronyms are the following: HYCOM = Hybrid Coordinate Ocean Model, MIT = Massachusetts Institute of Technology, MOM = Modular Ocean Model, NEMO = Nucleus for European Modelling of the Ocean, POM = Princeton Ocean Model, POP = Parallel Ocean Program, ROMS = Regional Ocean Modeling System.

smoothing. This result suggests that it is not just the horizontal pressure gradient error that has plagued terrain following models, but the additional interaction between numerically-induced mixing of active tracers and the pressure gradient.

### Where we stand with vertical coordinates

Table 5.1.1 provides a list of open source codes maintaining an active development process, providing updated and thorough documentation, and supporting an international user community. There are fewer codes listed in Table 5.1.1 than in the Griffies et al. (2000a) review written at the close of the WOCE era. It is inevitable that certain codes will not continue to be widely supported. There has also been a notable merger of efforts, such as in Europe where the majority of the larger modeling projects utilize the NEMO ocean component, and in the regional/shelf modeling community that focuses development on ROMS.

Numerical methods utilized for many of the community ocean codes have greatly improved during the past decade through intense development and a growing suite of applications. We are thus motivated to offer the following hypothesis.

PHYSICAL PARAMETERIZATIONS, MORE SO THAN VERTICAL COORDINATE, DETERMINE  
THE PHYSICAL INTEGRITY OF A GLOBAL OCEAN CLIMATE SIMULATION.



MODEL/INSTITUTE	WEB SITE
FESOM/AWI	<a href="http://www.awi.de/en">http://www.awi.de/en</a>
ICOM/Imperial	<a href="http://amcg.es.ee.ic.ac.uk/index.php?title=ICOM">http://amcg.es.ee.ic.ac.uk/index.php?title=ICOM</a>
ICON/MPI	<a href="http://www.mpimet.mpg.de/en/science/models/icon.html">http://www.mpimet.mpg.de/en/science/models/icon.html</a>
MPAS-ocean/LANL	<a href="http://public.lanl.gov/ringler/ringler.html">public.lanl.gov/ringler/ringler.html</a>
SLIM/Louvain	<a href="http://sites-final.uclouvain.be/slim/">http://sites-final.uclouvain.be/slim/</a>

Table 5.1.2: A non-exhaustive list of ongoing development efforts utilizing the flexibility of unstructured horizontal meshes. These efforts remain immature for large-scale climate applications, though there are some showing promise (e.g., Timmermann et al., 2009; Ringler et al., 2013). Furthermore, many efforts are not yet supporting open source public use due to their immaturity. Acronyms are the following: FESOM = Finite Element Sea-ice Ocean circulation Model, AWI = Alfred Wegener Institute for Polar and Marine Research in Germany, MPI = Max Planck Institute für Meteorologie in Germany, ICOM = Imperial College Ocean Model in the UK, MPAS = Model for Prediction Across Scales, LANL = Los Alamos National Laboratory in the USA, SLIM = Second-generation Louvain-la-Neuve Ice-ocean Model, Louvain = Louvain-la-Neuve in Belgium.

This hypothesis was untenable at the end of the WOCE era, which was the reason that Griffies et al. (2000a) emphasised vertical coordinates as the central defining feature of a model simulation. However, during the past decade, great strides in numerical methods have removed many of the “features” that distinguish large-scale simulations with different vertical coordinates. Hence, so long as the model configuration resolves flow features admitted by the simulation, there are fewer compelling reasons today than in the year 2000 to choose one vertical coordinate over another.

#### 5.1.2.8. UNSTRUCTURED HORIZONTAL GRID MESHES

Within the past decade, there has been a growing focus on unstructured horizontal meshes, based on finite volume or finite element methods. These approaches are very distinct from the structured Arakawa grids (Arakawa (1966), Arakawa & Lamb (1981)) used since the 1960s in both the atmosphere and ocean. The main motivation for generalization is to economically capture multiple scales seen in the ocean geometry (i.e., land-sea boundaries) and various scales of oceanic flow (i.e., boundary currents; coastal and shelf processes; active mesoscale eddy regimes). Griffies et al. (2010), Danilov (2013), and Ringler et al. (2013) review recent efforts with applications to the large-scale circulation.

There are many challenges facing finite element and unstructured finite volume methods. Even if the many technical issues listed in Section 4 of Griffies et al. (2010) are overcome, it remains unclear if these approaches will be computationally competitive with structured meshes. That is, more generality in grid meshing comes with a cost in added computational requirements. Nonetheless, the methods are sufficiently compelling to have motivated a new wave in efforts and to have entrained many smart minds towards seeing the ideas fully tested. Table 5.1.2 lists nascent efforts focused on aspects of this approach, with applications in the ocean. We anticipate that within 5-10 years, realistic coupled climate model simulations using unstructured ocean meshes will be realized.

### 810 5.1.3. Ocean modeling: science emerging from simulations

811 We now move from the reductionist theme focused on formulating a physically  
812 sound and numerically robust ocean model tool, to the needs of those aiming to use  
813 this tool for exploring wholistic questions of ocean circulation and climate. The basis  
814 for this exercise in *ocean modeling* is that the model tool has been formulated with  
815 sufficient respect to the fundamental physics so that simulated patterns and responses  
816 are physically meaningful. A successful ocean modeling activity thus requires a high  
817 fidelity numerical tool, a carefully designed experiment, and a variety of analysis meth-  
818 ods helping to unravel a mechanistic storyline.

819 We present a selection of topics relevant to the formulation of a numerical exper-  
820 iment aimed at understanding aspects of the global ocean circulation. Foremost is  
821 the issue of how to force an ocean or ocean-ice model. We rely for this discussion  
822 on the more thorough treatment given of global ocean-ice modeling in Griffies et al.  
823 (2009). In particular, we do not address the extremely difficult and ambiguous issues  
824 of model initialization and spinup, leaving such matters to the Griffies et al. (2009)  
825 paper for ocean-ice models and Chapter 5.4 of this volume for coupled climate models.  
826 Other important issues, such as boundary conditions for regional models and commu-  
827 nity model experiment strategies, are introduced very briefly. Additionally, we do not  
828 consider here the issues of fully coupled climate models (see Chapters 5.4, 5.5, and  
829 5.6).

#### 830 5.1.3.1. DESIGN CONSIDERATIONS FOR OCEAN-ICE SIMULATIONS

831 The ocean is a forced and dissipative system. Forcing occurs at the upper boundary  
832 from interactions with the atmosphere, rivers, sea ice, and land ice shelves, and at its  
833 lower boundary from the solid earth (see Figure 5.1.1). Forcing also occurs from astro-  
834 nomical effects of the sun and moon to produce tidal motions.<sup>1</sup> Important atmospheric  
835 forcing occurs over basin scales, with time scales set by the diurnal cycle, synoptic  
836 weather variability (days), the seasonal cycle, and inter-annual fluctuations such as the  
837 North Atlantic Oscillation and even longer time scales. Atmospheric momentum and  
838 buoyancy fluxes are predominantly responsible for driving the ocean’s large scale hori-  
839 zontal and overturning circulations (e.g., Kuhlbrodt et al., 2007). Additional influences  
840 include forcing at continental boundaries from river inflow and calving glaciers, as well  
841 as in polar regions where sea ice dynamics greatly affect the surface buoyancy fluxes.

842 Since the successes at reproducing the El Niño-Southern Oscillation phenomenon  
843 with linear ocean models in the early 1980s (Philander, 1990), a large number of forced  
844 ocean models have demonstrated skill in reproducing the main modes of tropical vari-  
845 ability without assimilation of in-situ ocean data, in part because of the linear character  
846 of the tropical ocean response to the winds (e.g., Illig et al. (2004)). Furthermore,  
847 studies from the past decade show that forced ocean models can, to some extent, repro-  
848 duce interannual ocean variability in mid-latitudes (e.g., regional patterns of decadal

---

<sup>1</sup>Climate modelers tend to ignore tidal forcing, but we may soon reach the limitations of assuming tidal motions merely add linearly to the low frequency solution (Schiller & Fiedler, 2007; Arbic et al., 2010).

849 sea level trends, Lombard et al. (2009)). Hence, a critical issue for the fidelity of an  
850 ocean and/or coupled ocean-ice simulation is the forcing methodology.

851 In the following, we introduce issues associated with how ocean models are forced  
852 through boundary fluxes. There is a spectrum of methods that go from the fully coupled  
853 climate models detailed in Chapter 5.4, to highly simplified boundary conditions such  
854 as damping of surface tracers to an “observed” dataset. Our focus is with ocean and  
855 ocean-ice models that are not coupled to an interactive atmosphere. Use of uncoupled  
856 ocean models allows one to remove biases inherent in the coupled climate models  
857 associated with the prognostic atmosphere component. Yet there is a price to pay when  
858 removing feedbacks. We outline these issues in the following.

### 859 **Air-sea flux formulation for coupled ocean-ice simulations**

860 Ice-ocean fluxes are not observed, and as a result ocean-ice coupled models are  
861 more commonly used than ocean-only models for investigations of the basin to global  
862 scale forced ocean circulation. Coupled ocean-ice models require surface momentum,  
863 heat, and hydrological fluxes to drive the simulated ocean and ice fields. When decou-  
864 pling the ocean and sea ice models from the atmosphere and land, one must introduce  
865 a method to generate these fluxes. One approach is to damp sea surface tempera-  
866 ture (SST) and salinity (SSS) to prescribed values. This approach for SST is sensible  
867 because SST anomalies experience a local negative feedback (Haney, 1971), whereby  
868 they are damped by interactions with the atmosphere. Yet the same is not true for salin-  
869 ity. Furthermore, the associated buoyancy fluxes generated by SST and SSS restoring  
870 can be unrealistic (Large et al. (1997), Killworth et al. (2000)). Barnier et al. (1995)  
871 introduced another method by combining prescribed fluxes and restoring. However,  
872 fluxes from observations and/or reanalysis products have large uncertainties (Taylor  
873 (2000), Large & Yeager (2004), Large & Yeager (2009), and Chapter 3.1 in this vol-  
874 ume), which can lead to unacceptable model drift (Rosati & Miyakoda, 1988).

875 Another forcing method prognostically computes turbulent fluxes for heat, mois-  
876 ture, and momentum from a planetary boundary layer scheme (Parkinson & Wash-  
877 ington (1979), Barnier (1998)), in addition to applying radiative heating, precipitation  
878 and river runoff. Turbulent fluxes are computed from bulk formulae as a function of  
879 the ocean surface state (SST and surface currents) and a prescribed atmospheric state  
880 (air temperature, humidity, sea level pressure, and wind velocity or wind speed). It is  
881 this approach that has been recommended by the CLIVAR Working Group for Ocean  
882 Model Development (WGOMD) for running *Coordinated Ocean-ice Reference Exper-*  
883 *iments* (COREs) (Griffies et al., 2009). Although motivated from its connection to  
884 fully coupled climate models, a fundamental limitation of this method relates to the  
885 use of a prescribed and nonresponsive atmospheric state that effectively has an infinite  
886 heat capacity, moisture capacity, and inertia.

887 The first attempts to define a forcing protocol for COREs have shown that a restor-  
888 ing to observed sea surface salinity is necessary to prevent multi-decadal drift in the  
889 ocean-ice simulations, even though such restoring has no physical basis (see Chapter  
890 6.2 as well as Rivin & Tziperman (1997)). It is thus desirable to use a weak restoring  
891 that does not prevent variability in the surface salinity and deep circulation. Unfor-  
892 tunately, when the restoring timescale for SSS is much longer than the effective SST  
893 restoring timescale, the thermohaline fluxes move into a regime commonly known as

894 *mixed boundary conditions* (Bryan, 1987), with rather unphysical sensitivities to buoy-  
895 ancy fluxes present in such regimes (Griffies et al., 2009). Furthermore, Griffies et al.  
896 (2009) have demonstrated that model solutions are very dependent on the arbitrary  
897 strength of the salinity restoring. Artificial salinity restoring may become unnecessary  
898 for short term simulations (a few years maximum), if the fidelity of ocean models and  
899 the observations of precipitation and runoff improve. For long term simulations, some  
900 way of parameterizing the missing feedback between evaporation and precipitation  
901 through atmospheric moisture transport is needed.

902 Another drawback of using a prescribed atmosphere to force an ocean-ice model  
903 is the absence of atmospheric response as the ice edge moves. Windy, cold, and dry  
904 air is often found near the sea ice edge in nature. Interaction of this air with the ocean  
905 leads to large fluxes of latent and sensible heat which cool the surface ocean, as well  
906 as evaporation which increases salinity. This huge buoyancy loss increases surface  
907 density, which provides a critical element in the downward branch of the thermohaline  
908 circulation (e.g., Marshall & Schott, 1999). When the atmospheric state is prescribed,  
909 where the simulated sea ice cover increases relative to the observed, the air-sea fluxes  
910 are spuriously shut down in the ocean-ice simulation.

#### 911 **Atmospheric datasets and continental runoff**

912 In order to be widely applicable in global ocean-ice modeling, an atmospheric  
913 dataset from which to derive surface boundary fluxes should produce near zero global  
914 mean heat and freshwater fluxes when used in combination with observed SSTs. This  
915 criteria precludes the direct use of atmospheric reanalysis products (see Chapter 3.1).  
916 As discussed in Taylor (2000), a combination of reanalysis and remote sensing prod-  
917 ucts provides a reasonable choice to force global ocean-ice models. Furthermore, it is  
918 desirable for many research purposes to provide both a repeating "normal" year forcing  
919 (NYF) as well as an interannually varying forcing. The dataset compiled by Large &  
920 Yeager (2004, 2009) satisfies these desires.

The Large & Yeager (2004, 2009) atmospheric state has been chosen for COREs.  
The most recent version of the dataset is available from

<http://data1.gfdl.noaa.gov/nomads/forms/core/COREv2.html>,

921 and it covers the period 1948 to 2009. It is based on NCEP-NCAR reanalysis tem-  
922 perature, wind and humidity, and satellite observations of radiation and precipitation  
923 (a climatology is used when satellite products are not available). Similar datasets have  
924 been developed by Röske (2006), and more recently by Brodeau et al. (2010), both  
925 of which are based on ECMWF products instead of NCEP. The Brodeau et al. (2010)  
926 dataset is used in the framework of the European Drakkar project (Drakkar Group,  
927 2007). The availability of multiple forcing datasets is useful in light of large uncertain-  
928 ties of air-sea fluxes. In addition, short term (i.e., interannual) or regional simulations  
929 can take advantage of other forcing data, such as scatterometer wind measurements,  
930 which have been shown to improve ocean simulations locally (Jiang et al., 2008).

931 For the multi-decadal global problem, further efforts are needed to improve the  
932 datasets used to force ocean models. For example, in the CORE simulations considered  
933 by Griffies et al. (2009), interannual variability of river runoff and continental ice melt

are not taken into account. However, recent efforts have incorporated both a seasonal cycle and interannually varying climatology into the river runoff, based on the Dai et al. (2009) analysis. Furthermore, the interpretation of trends in the forcing datasets is a matter of debate. For example, the increase of Southern Ocean winds between the early 1970s and the late 1990s is probably exaggerated in the atmospheric reanalyses due to the lack of Southern Ocean observations before 1979. This wind increase is retained in Large & Yeager (2009) used for COREs, whereas Brodeau et al. (2010) attempt to remove it for the Drakkar Forcing. These different choices lead, inevitably, to different decadal trends in the ocean simulations.

Considering the key role of polar regions and their high sensitivity to climate change, ocean-ice simulations will need improved forcings near the polar continents. One issue is taking into account the discharge of icebergs, which can provide a source of freshwater far from the continent, especially in the Antarctic (Jongma et al. (2009), Martin & Adcroft (2010)). The ice-ocean exchanges that occur due to the ocean circulation underneath the ice shelves is an additional complex process that needs to be taken into account, both for the purpose of modeling water mass properties near ice shelves and for the purpose of modeling the flow and stability of continental ice sheets (Chapter 4.6).

#### Wind stress, surface waves, and surface mixed layer

Mechanical work done by atmospheric winds provides a source of available potential energy that in turn drives much of the ocean circulation. A successful ocean simulation thus requires an accurate mechanical forcing. This task is far from trivial, not only because of wind uncertainties (reanalysis or scatterometer measurements) but also because of uncertainties in the transfer function between 10 meter wind vector and the air-sea wind stress. During the WOCE years, the wind stress was generally prescribed to force ocean models. However, with the generalization of the bulk approach led by Large & Yeager (2004, 2009), modelers started to use a bulk formula to compute the wind stress, with some choosing to do so as a function of the difference between the 10 m wind speed and the ocean velocity (Pacanowski, 1987). The use of such *relative winds* in the stress calculation has a significant damping effect on the surface eddy kinetic energy, up to 50% in the tropical Atlantic and about 10% in mid-latitudes (Eden & Dietze, 2009; Xu & Scott, 2008). Relative winds are clearly what the real system uses to exchange momentum between the ocean and atmosphere, so it is sensible to use such for coupled climate models where the atmosphere responds to the exchange of momentum with the ocean. However, we question the physical relevance of relative winds for the computation of stress in ocean-ice models, where the atmosphere is prescribed.

In general, the classical bulk formulae used to compute the wind stress are being questioned, given the complex processes relating surface wind, surface waves, ocean currents, and high frequency coupling with fine resolution atmosphere and ocean simulations (McWilliams & Sullivan, 2001; Sullivan et al., 2007; Sullivan & McWilliams, 2010). It is potentially important to take into account surface waves and swell not only in the wind stress formulation but also in the parameterization of vertical mixing in the surface boundary layer (Belcher et al., 2012).

### Boundary conditions for regional domains

In order to set up a numerical experiment in a regional domain, one needs to represent the lateral exchanges with the rest of the global ocean, at the “open” boundaries of the region of interest. When knowledge of the solution outside the simulated region is limited, an approach similar to the one advocated for ROMS is often used (Marchesiello et al., 2001). This method combines relaxation to a prescribed solution outside the domain with a radiation condition aimed at avoiding spurious reflection or trapping of perturbations at the open boundary. Treguier et al. (2001) have noted that in a realistic primitive equation model where Rossby waves, internal waves and turbulent eddies are present, the phase velocities calculated from the radiation condition have no relationship with the physical processes occurring at the boundary. Despite this fact, radiation appears to have a positive effect on the model solution, perhaps because it introduces stochastic noise in an otherwise over-determined problem. When the solution outside the domain is considered reliable, a “sponge” layer with relaxation to the outside solution is often preferred. Blayo & Debreu (2005) and Herzfeld et al. (2011) provide a review of various methods.

For the purpose of achieving regional simulations of good fidelity, the main progress accomplished in the past decade has come less from improved theory or numerics, and more from the availability of improved global model output that can be used to constrain the boundaries of regional models. These global datasets include operational products, ocean state estimates (Chapters 5.2 and 5.3) and prognostic global simulations (Barnier et al. (2006), Maltrud & McClean (2005)).

The quality of a regional model depends critically on the consistency between the solution outside and inside the domain. Consistency can be ensured by using the same numerical code for the global and regional solution; by using the same (or similar) atmospheric forcing; or by using strategies of grid refinement and nesting. Nesting can be one-way or two-way. For two-way, the large scale or global model is modified at each time step to fit the regional fine-scale solution. Although complex, two-way grid nesting is a promising strategy (Debreu & Blayo, 2008), with impressive applications documenting the role of Agulhas eddies in the variability of the Atlantic meridional overturning (Bjastoch et al., 2008). Further considerations are being given to nesting a number of fine resolution regions within a global model.

### Community model experiments

In Chapter 7.2 of the first edition of this book, Willebrand and Haidvogel wrote:

ONE THEREFORE CAN ARGUE THAT THE PRINCIPAL LIMITATION FOR MODEL DEVELOPMENT ARISES FROM THE LIMITED MANPOWER IN THE FIELD, AND THAT HAVING AN OVERLY LARGE MODEL DIVERSITY MAY NOT BE THE MOST EFFICIENT USE OF HUMAN RESOURCES. A MORE EFFICIENT WAY IS THE CONSTRUCTION OF *community models* THAT CAN BE USED BY MANY DIFFERENT GROUPS.

This statement seems prescient in regards to model codes, as noted by the reduced number of codes listed in Table 5.1.1 relative to the Griffies et al. (2000a) review. Additionally, it applies to the coordination of large simulation efforts. Indeed, WOCE has motivated the first Community Model Experiment (CME). This pioneering eddy permitting simulation of the Atlantic circulation (Bryan et al., 1995) and its companion

1022 sensitivity experiments have engaged a wide community of oceanographers. The re-  
 1023 sults gave insights into the origin of mesoscale eddies (Beckmann & Haidvogel, 1994),  
 1024 the mechanical energy balance (Treguier, 1992), and mechanisms driving the Atlantic  
 1025 meridional overturning circulation (Redler & Böning, 1997).

1026 As ocean model simulations refine their grid spacing over longer time periods,  
 1027 such community strategies become more useful, whereby simulations are performed  
 1028 in a coordinated fashion by a small group of scientists and distributed to a wider user  
 1029 community. An example of such strategy is carried out within the European DYNAMO  
 1030 project using regional models (Willebrand et al., 1997), and the more recent Drakkar  
 1031 project (Drakkar Group, 2007) that focuses on global ocean-ice models. Global hind-  
 1032 cast simulations of the past 50 years have been performed using the NEMO modeling  
 1033 framework for Drakkar (see Table 5.1.1), at different spatial resolutions from  $2^\circ$  to  
 1034  $1/12^\circ$ , with different forcings and model parameters. A few examples illustrate the  
 1035 usefulness of this approach.

- 1036 • Analyses of a hierarchy of global simulations with differing resolutions have  
 1037 revealed the role of mesoscale eddies in generating large scale, low frequency  
 1038 variability of sea surface height (SSH) (Penduff et al., 2010). Figure 5.1.4 shows  
 1039 that a significant part of the SSH variability observed at periods longer than 18  
 1040 months is not captured by the coarse resolution version of the model, but is re-  
 1041 produced in an eddy-permitting version, especially in western boundary currents  
 1042 and in the Southern Ocean.
- 1043 • Using experiments with different strategies for salinity restoring helped assess  
 1044 the robustness of modeled freshwater transports from the Arctic to the Atlantic  
 1045 (Lique et al., 2009).
- 1046 • A long experiment (obtained by cycling twice over the 50 years of forcing) with  
 1047 a  $1/4^\circ$  global model has been used to estimate the respective role of ocean heat  
 1048 transport and surface heat fluxes in variability of the Atlantic ocean heat content  
 1049 (Grist et al., 2010). The same simulation helped sort out the influence of model  
 1050 drift on the simulated response of the Antarctic Circumpolar Current to the recent  
 1051 increase in Southern ocean winds (Treguier et al., 2010).

#### 1052 5.1.3.2. ANALYSIS OF SIMULATIONS

1053 As models grow more realistic, they become tools of discovery. Important fea-  
 1054 tures of the ocean circulation have been discovered in models before being observed in  
 1055 nature. We highlight here two such discoveries.

- 1056 • ZAPIOLA ANTICYCLONE: The Zapiola anticyclone is a large barotropic circulation  
 1057 ( $\sim 100$  Sv) in the Argentine basin south of the Brazil-Malvinas confluence zone.  
 1058 It is a prominent feature in satellite maps of sea surface height variability (Fig-  
 1059 ure 5.1.5), causing a minimum of eddy activity located near  $45^\circ\text{S}$ ,  $45^\circ\text{W}$  inside  
 1060 a characteristic “C”-shaped maximum. The satellite record is now long enough  
 1061 to allow a detailed analysis of its variability (Volkov & Fu, 2008). This region  
 1062 is thus a key location for the evaluation of eddy processes represented in ocean  
 1063 circulation models.

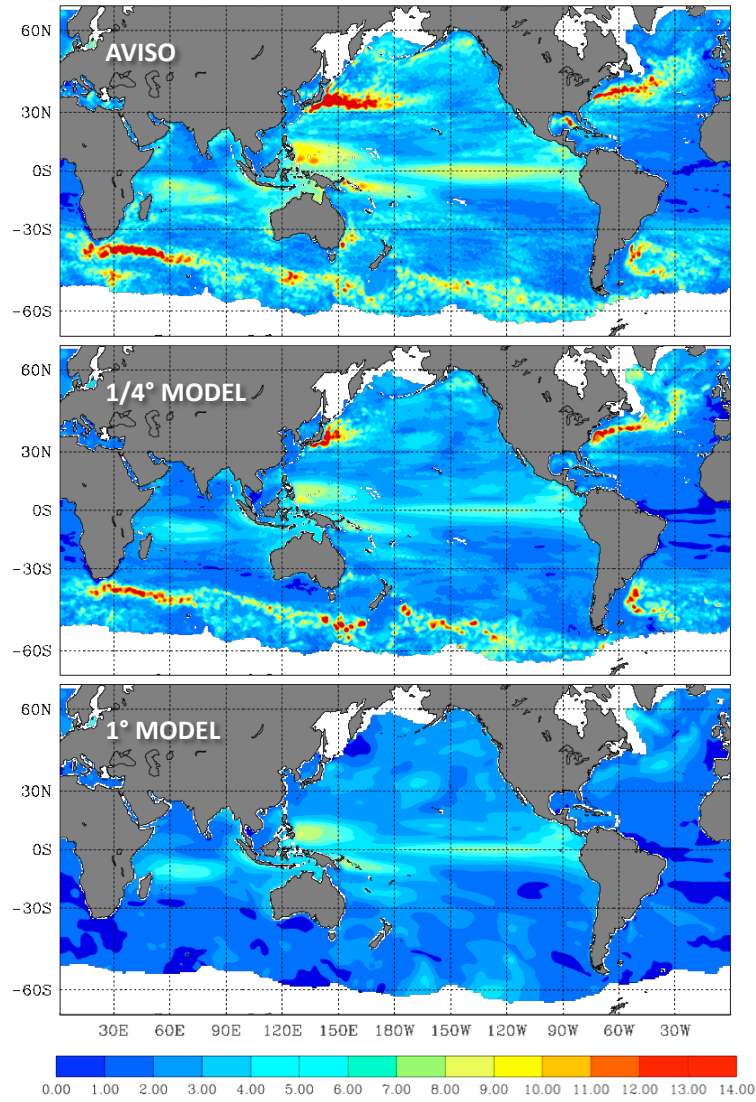


Figure 5.1.4: Variability of the sea surface height for periods longer than 18 months. Top: AVISO altimetric observations (Archiving, Validation, and Interpolation of Satellite Oceanographic; Le Traon et al. (1998); Ducet et al. (2000)); bottom panels: Drakkar model simulations at  $1/4^\circ$  and  $1^\circ$  horizontal grid spacing. Note the absence of much variability in the  $1^\circ$  simulation. Note the enhanced intrinsic ocean variability in the  $1/4^\circ$  model, in contrast to the one-degree model. See Penduff et al. (2010) for details of the models and the temporal filtering.

1064  
1065

The Zapiola anticyclone initially appeared in a terrain-following ocean model of the South Atlantic (B. Barnier, personal communication). Yet the circulation was



1066 considered a model artefact until observations confirmed its existence (Saunders  
1067 & King, 1995). As facilitated through studies with ocean models, the Zapiola  
1068 anticyclone arises from eddy-topography interactions (De Miranda et al., 1999).  
1069 More precisely, it results from a balance between eddy vorticity fluxes and dissipa-  
1070 tion, mainly due to bottom drag. For this reason, different models or different  
1071 numerical choices lead to different simulated strengths of this circulation (Fig-  
1072 ure 5.1.5).

1073 The Zapiola Drift rises 1100 m above the bottom of the Argentine Abyssal plain.  
1074 In model simulations that truncate the bottom to be no deeper than 5500 m,  
1075 the topographic seamount rises only 500 m above the maximum model depth,  
1076 whereas models with a maximum depth of 6000 m render a far more realistic  
1077 representation. Merryfield & Scott (2007) argue that the strength of the simu-  
1078 lated anticyclone can be dependent on the maximum depth in the model, with  
1079 shallower representations reducing the strength of the anticyclone.

- 1080 • **ZONAL JETS IN SOUTHWEST PACIFIC:** Another model-driven discovery is the exis-  
1081 tence of zonal jets in the Southwest Pacific, between 30°S and 10°S in the region  
1082 northeast of Australia. These jets, constrained by topography of the islands, were  
1083 first documented by the OCCAM eddy permitting model (Webb, 2000). Their  
1084 existence in the real ocean was later confirmed by satellite altimetry (Hughes,  
1085 2002).

1086 Whereas the science of ocean model development consists of the construction of  
1087 a comprehensive tool, the analysis of ocean simulations mechanistically deconstructs  
1088 and simplifies the output of the simulation to aid interpretation and to make connec-  
1089 tions to observations and theory. Analysis methods are prompted by the aims of the re-  
1090 search. For example, one may aim to develop a reduced or simplified description, with  
1091 dominant pieces of the physics identified to aid understanding and provoke further hy-  
1092 potheses, predictions, and theories. By doing so, understanding may arise concerning  
1093 how the phenomena emerges from the underlying physical laws, making simplifica-  
1094 tions where appropriate to remove less critical details and to isolate essential mech-  
1095 anisms. The following material represents a non-exhaustive selection of physically-  
1096 based analysis methods used in ocean modeling. It is notable that options for analyses  
1097 are enriched, and correspondingly more complex and computationally burdensome, as  
1098 the model resolution is refined to expand the admitted space and time scales, especially  
1099 when turbulent elements of the ocean mesoscale and finer scales are included.

1100 Our focus in the following concerns methods used to unravel elements of a particu-  
1101 lar simulation. To complement these methods, modelers often make use of perturbation  
1102 approaches whereby elements of the simulation are altered relative to a control case.  
1103 We have in mind those simulations that alter the boundary fluxes (e.g., remove buoy-  
1104 ancy and/or mechanical forcing, swap one forcing dataset for another, modify fluxes  
1105 over selected geographical regions); alter elements of the model’s prognostic equations  
1106 (e.g., modify subgrid scale parameterizations, remove nonlinear terms in the momen-  
1107 tum equation); and refine the horizontal and/or vertical grid spacing. When combined  
1108 with analysis methods such as those discussed below, these experimental approaches  
1109 are fundamental to why numerical models are useful for understanding the ocean.

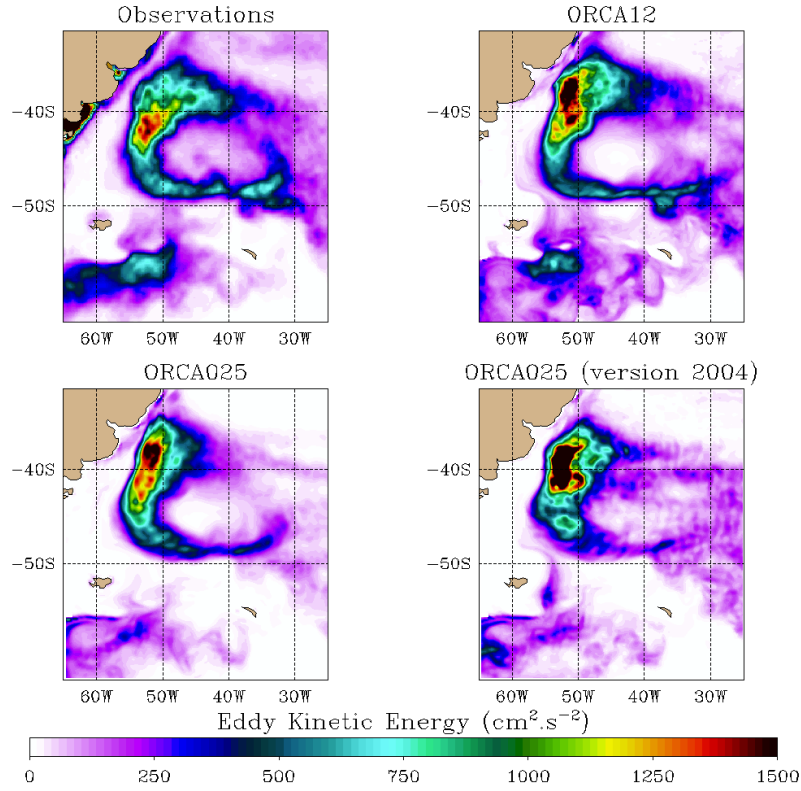


Figure 5.1.5: Variability of surface eddy kinetic energy (EKE) (units of  $\text{cm}^2 \text{s}^{-2}$ ) in the Argentine basin of the South Atlantic. (A): EKE of geostrophic currents calculated from altimetric observations (AVISO; Le Traon et al. (1998); Ducet et al. (2000)), based on 10-years mean (October 1992 until February 2002), (B) Drakkar ORCA12  $1/12^\circ$  global model, with simulated data taken from a 10-year mean (1998-2007: last 10 years of a multi-decade run), (C) recent version of the Drakkar ORCA025  $1/4^\circ$  global model, with simulated data taken from years 2000-2009 from a multi-decadal run, (D) same model as (C), but using an older model version with full step bathymetry and a different momentum advection scheme (referenced as ORCA025 G04 in Barnier et al. (2006)), with simulated data taken from 3-year mean (0008-0010: last 3 years from a climatological 10-year run). Note the good agreement with satellite measurements for both the ORCA12 and more recent ORCA025 simulations.

### Budget analysis

Identifying dominant terms in the tracer, momentum, and/or vorticity budgets assists in the quest to develop a reduced description, which in turn isolates what physical processes are essential. The straightforward means for doing so consists of a budget analysis, which generally occurs within the framework of the model equations associated with the finite volume budgets as developed in Section 5.1.2.4.

As one example, the mechanical energy cycle of the ocean has been the subject of interest since a series of papers pointed out the potential role of diapycnal mixing as a

key energy source for the overturning circulation (Wunsch & Ferrari, 2004; Kuhlbrodt et al., 2007). This work has motivated model-based studies aimed at understanding the energy cycle of the ocean. For example, Gnanadesikan et al. (2005) demonstrated that the link between mechanical mixing and meridional heat transport is rather weak in a climate model with parameterized ocean mesoscale eddies. No unifying view has emerged, but the approach is promising, and will gain momentum when results can be confirmed in more refined eddying global models.

Other examples include budgets of heat or salt in key regions, such as the surface mixed layer (Vialard & Delecluse, 1998) or the subtropical waters (McWilliams et al., 1996). Griffies & Greatbatch (2012) and Palter et al. (2013) present detailed budget analyses focusing on the role of buoyancy on global and regional sea level. Following the pioneering studies of the 1990s, a large number of model-based analyses have considered such tracer budgets in various parts of the ocean. The Argo observing network now makes possible similar analyses that can be partially compared with model results (e.g., de Boisseson et al. (2010)). The confrontation of model-based and observation-based tracer budgets will undoubtedly help improve the representation of mixing processes in models.

### Isopycnal watermass analysis

How much seawater or tracer transport passes through an isopycnal layer is a common question asked of model analysts. Relatedly, isopycnal mass analysis as per methods of Walin (1982) have proven of use for inferring the amount of watermass transformation associated with surface boundary fluxes (e.g., Tziperman (1986), Speer & Tziperman (1992), Williams et al. (1995), Marshall et al. (1999), Large & Nurser (2001), Maze et al. (2009), Downes et al. (2011)). Numerical models allow one to go beyond an analysis based solely on surface fluxes, so that interior transformation processes can be directly deduced. For example, the effect of mesoscale eddies on the subduction from the surface mixed layer into the ocean interior has been quantified in the North Atlantic (Costa et al., 2005). By performing a full three-dimensional analysis in a neutral density framework, Iudicone et al. (2008) discovered the essential importance of light penetration on the formation of tropical water masses.

### Lagrangian analysis

The Lagrangian parcel perspective often provides useful complementary information relative to the more commonly used Eulerian (fixed point) perspective. One method of Lagrangian analysis proposed by Blanke et al. (1999), as well as Vries & Döös (2001) and van Sebille et al. (2009), uses mass conservation (or volume conservation in Boussinesq models) to decompose mass transport into a large number of “particles”, each carrying a tiny fraction of the transport. By following these particles using a Lagrangian algorithm, one can recover the transport of water masses and diagnose their transformation.

Applications of such Lagrangian analyses are numerous. Examples include the tropical Atlantic study of Blanke et al. (1999); the first quantification of the contribution of the Tasman leakage to the global conveyor belt (Speich et al., 2002); the Lagrangian view of the meridional circulation in the Southern Ocean (Döös et al., 2008; Iudicone et al., 2011); and quantification of how water masses are transferred between different

regions (Rodgers et al. (2003), Koch-Larrouy et al. (2008), Melet et al. (2011)). These Lagrangian methods have been applied to models absent mesoscale eddies, or only partially admitting such eddies, where a significant part of the dispersion of water masses is parameterized rather than explicitly resolved. The application to eddy models requires large computer resources, and thus have to date only been applied in regional models (Melet et al., 2011). More classical Lagrangian analysis, following arbitrary parcels without relation to the mass transports, have also been applied to eddy models, with a focus on statistical analyses of dispersion (Veneziani et al., 2005).

### Passive tracer methods

Many of the ocean's trace constituents have a negligible impact on ocean density, in which case these tracers are dynamically passive (Chapter 5.7). England & Maier-Reimer (2001) review how chemical tracers, such as CFCs and radioactive isotopes, can be used to help understand both the observed and simulated ocean circulation, largely by providing means of tracking parcel motions as well as diagnosing mixing processes. Purposefully released tracers have provided benchmarks for measurements of mixing across the ocean thermocline and abyss (Ledwell et al., 1993; Ledwell & Watson, 1998; Ledwell et al., 2011). Ocean modelers have used similar tracer methods to assess physical and spurious numerical mixing (Section 5.1.2.6). Tracers can also provide estimates for the time it takes water to move from one region to another, with such timescale or generalized age methods exemplified by the many articles in Deleersnijder et al. (2010).

#### 5.1.4. Summary remarks

The evolution of numerical methods, physical parameterizations, and ocean climate applications has been substantial since the first edition of this book in 2001. Today, we better understand the requirements of, for example, maintaining a realistic tropical thermocline essential for simulations of El Niño fluctuations (Meehl et al., 2001), whereas earlier models routinely suffered from an overly diffuse thermocline. We understand far more about the importance of and sensitivity to various physical parameterizations, such as mixing induced by breaking internal waves (Chapter 3.3) and lateral mixing/stirring from mesoscale and submesoscale eddies (Chapter 3.4). Nonetheless, many of the key questions from the first edition remain with us today, in part because the ocean “zoo” (Figure 5.1.1) is so diverse and difficult to tame.

Questions about resolution of physical processes and/or their parameterization sit at the foundation of nearly all compelling questions of ocean models and modeling. What does it mean to fully resolve a physical process? What sorts of numerical methods and/or vertical coordinates are appropriate? Are the multi-scale methods offered by unstructured meshes an optimal means for representing and parameterizing (using scale aware schemes) the multi-scales of ocean fluid dynamics and fractal structure of the land-sea geometry? How well does a parameterization support high fidelity simulations? How do we parameterize a process that is partially resolved without suppressing and/or double-counting those elements of the process that are resolved? Relatedly, how do subgrid scale parameterizations impact on an *effective* resolution? What are the climate impacts from a particular physical process? Are these impacts robust to whether

1205 the process is unresolved and parameterized, partially resolved and partially parameter-  
1206 ized, or fully resolved? We suggested potential avenues in pursuit of answers to these  
1207 questions, though noted that robust answers will perhaps only be available after global  
1208 climate models routinely resolve processes to determine their role in a holistic context.

1209 Amongst the most important transitions to have occurred during the past decade is  
1210 the growing presence of mesoscale eddying global ocean climate simulations. Changes  
1211 may appear in air-sea fluxes in coupled simulations due to refined representation of  
1212 frontal-scale features (Bryan et al., 2010); circulation can be modified through eddy-  
1213 mean flow interactions (Holland & Rhines, 1980); stochastic features are introduced  
1214 through eddy fluctuations; and currents interact with a refined representation of bathymetry.  
1215 Relative to their more laminar predecessors, eddying simulations necessitate enhanced  
1216 fidelity from numerical methods and require a wide suite of analysis methods to un-  
1217 ravel mechanisms. There is progress, but more is required before mesoscale eddying  
1218 simulations achieve the trust and familiarity required to make them a robust scientific  
1219 tool for numerical oceanography and climate. In particular, we need a deeper under-  
1220 standing of the generation and decay of mesoscale eddies, both to ensure their proper  
1221 representation in eddying simulations, and to parameterize in coarse models. We also  
1222 must address the difficulties associated with managing the huge amounts of simulated  
1223 data generated by global eddying simulations.

1224 No sound understanding exists of what is required from both grid spacing and nu-  
1225 merical methods to fully resolve the mesoscale in global models. The work of Smith  
1226 et al. (2000) suggest that the mesoscale is resolved so long as the grid spacing is finer  
1227 than the first baroclinic Rossby radius. This is a sensible hypothesis given that the  
1228 mesoscale eddy scales are proportional to the Rossby radius, and given that much of  
1229 the mid-latitude ocean energy is contained in the barotropic and first baroclinic modes.  
1230 However, this criterion was proposed without a rigorous examination of how important  
1231 higher modes may be; how sensitive this criteria is to specifics of numerical methods  
1232 and subgrid scale parameterizations; or whether the criteria is supported by a thorough  
1233 resolution study. We propose that a solid understanding of the mesoscale eddy resolu-  
1234 tion question will greatly assist in answering many of the questions regarding the role  
1235 of the ocean in climate.

1236 A related question concerns the relation between the numerical modeling of mesoscale  
1237 eddies and diapycnal mixing. Namely, is it sensible to consider mesoscale eddying cli-  
1238 mate simulations using a model that includes unphysically large spurious diapycnal  
1239 mixing? Are isopycnal models, or their generalizations to ALE (Arbitrary Lagrangian-  
1240 Eulerian) methods, the optimal means for ensuring spurious numerical mixing is suffi-  
1241 ciently small to accurately capture physical mixing processes, even in the presence of  
1242 realistic stirring from mesoscale eddies? Or will the traditional level model approaches  
1243 be enhanced sufficiently to make the modeler’s choice based on convenience rather  
1244 than fundamentals? We conjecture that an answer will be clear within a decade.

1245 As evidenced by the increasing “operational” questions being asked by oceanogra-  
1246 phers, spanning the spectrum from real time ocean forecasting (Chapter 5.3) to interan-  
1247 nual to longer term climate projections (Chapters 5.4, 5.5, 5.6, 5.7) as well as reanalysis  
1248 and state estimation (Chapter 5.2), numerical oceanography is being increasingly asked  
1249 to address applied questions that have an impact on decisions reaching outside of sci-  
1250 ence. As with the atmospheric sciences, the added responsibility, and the associated

1251 increased visibility, arising from applications brings great opportunities for enhancing  
1252 ocean science. The increased functionality and applications of ocean models must in  
1253 turn be strongly coupled to a continued focus on the physics and numerics forming  
1254 their foundation.

## 1255 **Acknowledgements**

1256 We thank WCRP/CLIVAR for sponsoring the Working Group for Ocean Model  
1257 Development, where the authors have participated since 1999. The presentation in this  
1258 chapter was greatly assisted by comments from John Church, Carolina Dufour, John  
1259 Gould, Trevor McDougall, Angélique Melet, Maxim Nikurashin, Gerold Siedler, and  
1260 an anonymous reviewer. Bernard Barnier kindly provided the Drakkar/ORCA simula-  
1261 tion results for Figure 5.1.5. Cathy Raphael kindly drafted Figure 5.1.1.

## 1262 **References**

- 1263 Adcroft, A., & Campin, J.-M. (2004). Rescaled height coordinates for accurate rep-  
1264 resentation of free-surface flows in ocean circulation models. *Ocean Modelling*, 7,  
1265 269–284.
- 1266 Adcroft, A., Hallberg, R., Dunne, J., Samuels, B., Galt, J., Barker, C., & Payton, D.  
1267 (2010). Simulations of underwater plumes of dissolved oil in the Gulf of Mexico.  
1268 *Geophysical Research Letters*, doi:10.1029/2010GL044689.
- 1269 Adcroft, A., & Hallberg, R. W. (2006). On methods for solving the oceanic equations  
1270 of motion in generalized vertical coordinates. *Ocean Modelling*, 11, 224–233.
- 1271 Adcroft, A., Hill, C., & Marshall, J. (1997). Representation of topography by shaved  
1272 cells in a height coordinate ocean model. *Monthly Weather Review*, 125, 2293–2315.
- 1273 Adcroft, A., Scott, J. R., & Marotzke, J. (2001). Impact of geothermal heating on the  
1274 global ocean circulation. *Geophysical Research Letters*, 28, 1735–1738.
- 1275 Arakawa, A. (1966). Computational design for long-term numerical integration of the  
1276 equations of fluid motion: Two-dimensional incompressible flow. Part 1. *Journal of*  
1277 *Computational Physics*, 1, 119–143.
- 1278 Arakawa, A., & Lamb, V. (1981). A potential enstrophy and energy conserving scheme  
1279 for the shallow water equations. *Monthly Weather Review*, 109, 18–36.
- 1280 Arbic, B., Wallcraft, A., & Metzger, E. (2010). Concurrent simulation of the eddying  
1281 general circulation and tides in a global ocean model. *Ocean Modelling*, 32, 175–  
1282 187.

- 1283 Barnier, B. (1998). Forcing the ocean. In E. P. Chassignet, & J. Verron (Eds.), *Ocean*  
1284 *Modeling and Parameterization* (pp. 45–80). Kluwer volume 516 of *NATO ASI*  
1285 *Mathematical and Physical Sciences Series*.
- 1286 Barnier, B., Madec, G., Penduff, T., Molines, J., Treguier, A., Sommer, J. L., Beck-  
1287 mann, A., Biastoch, A., Böning, C. W., Dengg, J., Derval, C., Durand, E., Gulev, S.,  
1288 Remy, E., Talandier, C., Theetten, S., Maltrud, M., McClean, J., & Cuevas, B. D.  
1289 (2006). Impact of partial steps and momentum advection schemes in a global ocean  
1290 circulation model at eddy permitting resolution. *Ocean Dynamics*, 56, 543–567.
- 1291 Barnier, B., Siefridt, L., & Marchesiello, P. (1995). Thermal forcing for a global ocean  
1292 circulation model using a three-year climatology of ECMWF analyses. *Journal of*  
1293 *Marine Research*, 6, 363–380.
- 1294 Bates, M., Griffies, S. M., & England, M. (2012a). A dynamic, embedded Lagrangian  
1295 model for ocean climate models, Part I: Theory and implementation. *Ocean Mod-*  
1296 *elling*, .
- 1297 Bates, M., Griffies, S. M., & England, M. (2012b). A dynamic, embedded Lagrangian  
1298 model for ocean climate models, Part II: Idealised overflow tests. *Ocean Modelling*,  
1299 .
- 1300 Beckmann, A. (1998). The representation of bottom boundary layer processes in nu-  
1301 merical ocean circulation models. In E. P. Chassignet, & J. Verron (Eds.), *Ocean*  
1302 *Modeling and Parameterization* (pp. 135–154). Kluwer volume 516 of *NATO ASI*  
1303 *Mathematical and Physical Sciences Series*.
- 1304 Beckmann, A., & Döscher, R. (1997). A method for improved representation of dense  
1305 water spreading over topography in geopotential-coordinate models. *Journal of*  
1306 *Physical Oceanography*, 27, 581–591.
- 1307 Beckmann, A., & Haidvogel, D. (1993). Numerical simulation of flow around a tall iso-  
1308 lated seamount. Part I: Problem formulation and model accuracy. *Journal of Physical*  
1309 *Oceanography*, 23, 1736–1753.
- 1310 Beckmann, A., & Haidvogel, D. (1994). On the generation and role of eddy variability  
1311 in the central North Atlantic Ocean. *Journal of Geophysical Research*, 99, 20381–  
1312 20391.
- 1313 Belcher, S., Grant, A., Hanley, K., Fox-Kemper, B., Van Roekel, L., Sullivan, P., Large,  
1314 W., Brown, A., Hines, A., Calvert, D., Rutgersson, A., Petterson, H., Bidlot, J.,  
1315 Janssen, P., & Polton, J. A. (2012). A global perspective on Langmuir turbulence  
1316 in the ocean surface boundary layer. *Geophysical Research Letters*, 39-L18605,  
1317 doi:10.1029/2012GL052932.
- 1318 Berlov, P. (2005). Random-forcing model of the mesoscale oceanic eddies. *Journal of*  
1319 *Fluid Mechanics*, 529, 71–95.
- 1320 Biastoch, A., Böning, C., & Lutjeharms, J. (2008). Agulhas leakage dynamics affects  
1321 decadal variability in Atlantic overturning circulation. *Nature*, 456:7221, 489–492.

- 1322 Blanke, B., Arhan, M., Madec, G., & Roche, S. (1999). Warm water paths in the equa-  
1323 torial Atlantic as diagnosed with a general circulation model. *Journal of Physical*  
1324 *Oceanography*, 29, 2753–2768.
- 1325 Blayo, E., & Debreu, L. (2005). Revisiting open boundary conditions from the point  
1326 of view of characteristic variables. *Ocean Model.*, 9, 231–252.
- 1327 Bleck, R. (1998). Ocean modeling in isopycnic coordinates. In E. P. Chassignet, &  
1328 J. Verron (Eds.), *Ocean Modeling and Parameterization* (pp. 423–448). Kluwer  
1329 volume 516 of *NATO ASI Mathematical and Physical Sciences Series*.
- 1330 Bleck, R. (2002). An oceanic general circulation model framed in hybrid isopycnic-  
1331 cartesian coordinates. *Ocean Modelling*, 4, 55–88.
- 1332 Boccaletti, G., Ferrari, R., & Fox-Kemper, B. (2007). Mixed layer instabilities and  
1333 restratification. *Journal of Physical Oceanography*, 35, 1263–1278.
- 1334 de Boisseson, E., Thierry, V., Mercier, H., & Caniaux, G. (2010). Mixed layer heat bud-  
1335 get in the iceland basin from argo. *Journal of Geophysical Research*, 115, C10055.
- 1336 Böning, C. W., Dispert, A., Visbeck, M., Rintoul, S., & Schwarzkopf, F. (2008). The  
1337 response of the Antarctic Circumpolar Current to recent climate change. *Nature*  
1338 *Geoscience*, 1, 864–869.
- 1339 Brankart, J.-M. (2013). Impact of uncertainties in the horizontal density gradient upon  
1340 low resolution global ocean modelling. *Ocean Modelling*, *submitted*.
- 1341 Brodeau, L., Barnier, B., Treguier, A., Penduff, T., & Gulev, S. (2010). An ERA40-  
1342 based atmospheric forcing for global ocean circulation models. *Ocean Modelling*,  
1343 31, 88–104.
- 1344 Bryan, F. (1987). Parameter sensitivity of primitive equation ocean general circulation  
1345 models. *Journal of Physical Oceanography*, 17, 970–985.
- 1346 Bryan, F., Böning, C., & Holland, W. (1995). On the mid-latitude circulation in a  
1347 high resolution model of the North Atlantic. *Journal of Physical Oceanography*, 25,  
1348 289–305.
- 1349 Bryan, F., Thomas, R., Dennis, J., Chelton, D., Loeb, N., & McClean, J. (2010). Frontal  
1350 scale air-sea interaction in high-resolution coupled climate models. *Journal of Cli-*  
1351 *mate*, 23, 6277–6291.
- 1352 Bryan, K., & Lewis, L. J. (1979). A water mass model of the world ocean. *Journal of*  
1353 *Geophysical Research*, 84, 2503–2517.
- 1354 Bryan, K., Manabe, S., & Pacanowski, R. C. (1975). A global ocean-atmosphere cli-  
1355 mate model. Part II. The oceanic circulation. *Journal of Physical Oceanography*, 5,  
1356 30–46.
- 1357 Campin, J.-M., & Goosse, H. (1999). Parameterization of density-driven downsloping  
1358 flow for a coarse-resolution ocean model in  $z$ -coordinate. *Tellus*, 51A, 412–430.



- 1359 Campin, J.-M., Marshall, J., & Ferreira, D. (2011). Super-parameterization in ocean  
1360 modeling: Application to deep convection. *Ocean Modelling*, 36, 90–101.
- 1361 Cavaleri, L., Fox-Kemper, B., & Hemer, M. (2012). Wind waves in the coupled climate  
1362 system. *Bulletin of the American Meteorological Society*, 93, 1651–1661.
- 1363 Chaikin, P. M., & Lubensky, T. C. (1995). *Principles of Condensed Matter Physics*.  
1364 Cambridge, United Kingdom: Cambridge University Press.
- 1365 Costa, M. D., Mercier, H., & Treguier, A.-M. (2005). Effects of the mixed layer time  
1366 variability on kinematic subduction rate diagnostics. *Journal of Physical Oceanog-*  
1367 *raphy*, 35, 427–443.
- 1368 Cox, M. D. (1984). *A Primitive Equation, 3-Dimensional Model of the Ocean*. Prince-  
1369 ton, USA: NOAA/Geophysical Fluid Dynamics Laboratory.
- 1370 Dai, A., Qian, T., Trenberth, K., & Milliman, J. (2009). Changes in continental fresh-  
1371 water discharge from 1948–2004. *Journal of Climate*, 22, 2773–2791.
- 1372 Danabasoglu, G., Large, W., & Briegleb, B. (2010). Climate impacts of param-  
1373 eterized nordic sea overflows. *Journal of Geophysical Research*, 115, C11005,  
1374 doi:10.1029/2010JC006243.
- 1375 Danilov, S. D. (2013). Ocean modeling on unstructured meshes. *Ocean Modelling*, ...,  
1376 doi.org/10.1016/j.ocemod.2013.05.005.
- 1377 Davis, R. E. (1994a). Diapycnal mixing in the ocean: equations for large-scale budgets.  
1378 *Journal of Physical Oceanography*, 24, 777–800.
- 1379 Davis, R. E. (1994b). Diapycnal mixing in the ocean: the Osborn-Cox model. *Journal*  
1380 *of Physical Oceanography*, 24, 2560–2576.
- 1381 De Miranda, A., Barnier, B., & Dewar, W. (1999). On the dynamics of the Zapiola  
1382 Anticyclone. *Journal of Geophysical Research*, 104, 21137–21149.
- 1383 Debreu, L., & Blayo, E. (2008). Two-way embedding algorithms: a review. *Ocean*  
1384 *Dynamics*, 58, 415–428.
- 1385 DeGroot, S. R., & Mazur, P. (1984). *Non-Equilibrium Thermodynamics*. New York:  
1386 Dover Publications. 510 pp.
- 1387 Deleersnijder, E., & Beckers, J.-M. (1992). On the use of the  $\sigma$ -coordinate system in  
1388 regions of large bathymetric variations. *Journal of Marine Systems*, 3, 381–390.
- 1389 Deleersnijder, E., Cornaton, F., Haine, T., Vanclooster, M., & Waugh, D. W. (2010).  
1390 Tracer and timescale methods for understanding complex geophysical and environ-  
1391 mental fluid flows. *Environmental Fluid Mechanics*, 10, DOI 10.1007/s10652-009-  
1392 9164-1.

- 1393 Delworth, T. L., Rosati, A., Anderson, W., Adcroft, A. J., Balaji, V., Benson, R., Dixon,  
1394 K., Griffies, S. M., Lee, H.-C., Pacanowski, R. C., Vecchi, G. A., Wittenberg, A. T.,  
1395 Zeng, F., & Zhang, R. (2012). Simulated climate and climate change in the GFDL  
1396 CM2.5 high-resolution coupled climate model. *Journal of Climate*, 25, 2755–2781.
- 1397 Denbo, D., & Skillingstad, E. (1996). An ocean large-eddy simulation model with ap-  
1398 plication to deep convection in the Greenland Sea. *Journal of Geophysical Research*,  
1399 101, 1095–1110.
- 1400 DeSzoek, R. A. (2009). Isentropic averaging. *Journal of Marine Research*, 67, 533–  
1401 567.
- 1402 DeSzoek, R. A., & Bennett, A. F. (1993). Microstructure fluxes across density sur-  
1403 faces. *Journal of Physical Oceanography*, 23, 2254–2264.
- 1404 DeSzoek, R. A., & Samelson, R. M. (2002). The duality between the Boussinesq and  
1405 non-Boussinesq hydrostatic equations of motion. *Journal of Physical Oceanogra-  
1406 phy*, 32, 2194–2203.
- 1407 Dietrich, D., Marietta, M., & Roache, P. (1987). An ocean modeling system with  
1408 turbulent boundary layers and topography: Part 1. numerical studies of small island  
1409 wakes in the ocean. *International Journal of Numerical Methods in Fluids*, 7, 833–  
1410 855.
- 1411 Donea, J., Huerta, A., Ponthot, J.-P., & Rodríguez-Ferran, A. (2004). Arbitrary  
1412 Lagrangian-Eulerian methods. In E. Stein, R. de Borst, & T. J. R. Hughes (Eds.),  
1413 *Encyclopedia of Computational Mechanics* chapter 14. John Wiley and Sons.
- 1414 Döös, K., Nycander, J., & Coward, A. (2008). Lagrangian decomposition of the Dea-  
1415 con Cell. *Journal of Geophysical Research-Oceans*, 113.
- 1416 Downes, S. M., Gnanadesikan, A., Griffies, S. M., & Sarmiento, J. (2011). Water mass  
1417 exchange in the Southern Ocean in coupled climate models. *Journal of Physical  
1418 Oceanography*, 41, 1756–1771.
- 1419 Drakkar Group (2007). Eddy-permitting ocean circulation hindcasts of past decades.  
1420 *CLIVAR Exchanges*, 42, 8–10.
- 1421 Ducet, N., Le Traon, P.-Y., & Reverdin, G. (2000). Global high-resolution mapping of  
1422 ocean circulation from TOPEX/Poseidon and ERS-1 and -2. *Journal of Geophysical  
1423 Research*, 105, 19477–19498.
- 1424 Dunne, J. P., John, J. G., Hallberg, R. W., Griffies, S. M., Shevliakova, E. N., Stouffer,  
1425 R. J., Krasting, J. P., Sentman, L. A., Milly, P. C. D., Malyshev, S. L., Adcroft, A. J.,  
1426 Cooke, W., Dunne, K. A., Harrison, M. J., Levy, H., Samuels, B. L., Spelman, M.,  
1427 Winton, M., Wittenberg, A. T., Phillips, P. J., & Zadeh, N. (2012). GFDLs ESM2  
1428 global coupled climate-carbon Earth System Models Part I: Physical formulation  
1429 and baseline simulation characteristics. *Journal of Climate*, 25, 6646–6665.

- 1430 Eckart, C. (1948). An analysis of the stirring and mixing processes in incompressible  
1431 fluids. *Journal of Marine Research*, 7, 265–275.
- 1432 Eden, C., & Dietze, H. (2009). Effects of mesoscale eddy/wind interactions on biolog-  
1433 ical new production and eddy kinetic energy. *Journal of Geophysical Research*, 114,  
1434 C05023.
- 1435 Eden, C., Greatbatch, R., & Olbers, D. (2007). Interpreting eddy fluxes. *Journal of*  
1436 *Physical Oceanography*, 37, 1282–1296.
- 1437 Emile-Geay, J., & Madec, G. (2009). Geothermal heating, diapycnal mixing and the  
1438 abyssal circulation. *Ocean Science*, 5, 203–217.
- 1439 England, M. H., & Maier-Reimer, E. (2001). Using chemical tracers to assess ocean  
1440 models. *Reviews of Geophysics*, 39, 29–70.
- 1441 Farneti, R., Delworth, T., Rosati, A., Griffies, S. M., & Zeng, F. (2010). The role  
1442 of mesoscale eddies in the rectification of the Southern Ocean response to climate  
1443 change. *Journal of Physical Oceanography*, 40, 1539–1557.
- 1444 Farneti, R., & Gent, P. (2011). The effects of the eddy-induced advection coefficient in  
1445 a coarse-resolution coupled climate model. *Ocean Modelling*, 39, 135–145.
- 1446 Fox-Kemper, B., Ferrari, R., & Hallberg, R. (2008). Parameterization of mixed layer  
1447 eddies. I: Theory and diagnosis. *Journal of Physical Oceanography*, 38, 1145–1165.
- 1448 Fox-Kemper, B., & Menemenlis, D. (2008). Can large eddy simulation techniques  
1449 improve mesoscale rich ocean models? In M. Hecht, & H. Hasumi (Eds.), *Eddy re-*  
1450 *solving ocean models* Geophysical Monograph 177 (pp. 319–338). American Geo-  
1451 physical Union.
- 1452 Frankignoul, C., & Hasselmann, K. (1977). Stochastic climate models. Part II: Appli-  
1453 cation to sea-surface temperature variability and thermocline variability. *Tellus*, 29,  
1454 284–305.
- 1455 Gent, P., & Danabasoglu, G. (2011). Response of increasing Southern Hemisphere  
1456 winds in CCSM4. *Journal of Climate*, 24, 4992–4998.
- 1457 Gent, P. R., & McWilliams, J. C. (1990). Isopycnal mixing in ocean circulation models.  
1458 *Journal of Physical Oceanography*, 20, 150–155.
- 1459 Gent, P. R., Willebrand, J., McDougall, T. J., & McWilliams, J. C. (1995). Parameteriz-  
1460 ing eddy-induced tracer transports in ocean circulation models. *Journal of Physical*  
1461 *Oceanography*, 25, 463–474.
- 1462 Gill, A. (1982). *Atmosphere-Ocean Dynamics* volume 30 of *International Geophysics*  
1463 *Series*. London: Academic Press. 662 + xv pp.
- 1464 Gnanadesikan, A., Slater, R. D., Swathi, P. S., & Vallis, G. K. (2005). The energetics  
1465 of ocean heat transport. *Journal of Climate*, 17, 2604–2616.

- Goldberg, D., Little, C., Sergienko, O., Gnanadesikan, A., Hallberg, R., & Oppenheimer, M. (2012). Investigation of land ice-ocean interaction with a fully coupled ice-ocean model: 1. Model description and behavior. *Journal of Geophysical Research*, 117-F02037, doi:10.1029/2011JF002246.
- Grabowski, W. (2001). Coupling cloud processes with the large-scale dynamics using the Cloud-Resolving Convection Parameterization (CRCP). *Journal of Atmospheric Sciences*, 58, 978–997.
- Greatbatch, R. J. (1994). A note on the representation of steric sea level in models that conserve volume rather than mass. *Journal of Geophysical Research*, 99, 12767–12771.
- Greatbatch, R. J., & McDougall, T. J. (2003). The non-Boussinesq temporal-residual-mean. *Journal of Physical Oceanography*, 33, 1231–1239.
- Gregg, M., Sanford, T., & Winkel, D. (2003). Reduced mixing from the breaking of internal waves in equatorial waters. *Nature*, 422, 513–515.
- Griffies, S. M. (1998). The Gent-McWilliams skew-flux. *Journal of Physical Oceanography*, 28, 831–841.
- Griffies, S. M. (2004). *Fundamentals of Ocean Climate Models*. Princeton, USA: Princeton University Press. 518+xxxiv pages.
- Griffies, S. M., & Adcroft, A. J. (2008). Formulating the equations for ocean models. In M. Hecht, & H. Hasumi (Eds.), *Eddy resolving ocean models* Geophysical Monograph 177 (pp. 281–317). American Geophysical Union.
- Griffies, S. M., Adcroft, A. J., Banks, H., Böning, C. W., Chassignet, E. P., Danabasoglu, G., Danilov, S., Deleersnijder, E., Drange, H., England, M., Fox-Kemper, B., Gerdes, R., Gnanadesikan, A., Greatbatch, R. J., Hallberg, R., Hanert, E., Harrison, M. J., Legg, S. A., Little, C. M., Madec, G., Marsland, S., Nikurashin, M., Pirani, A., Simmons, H. L., Schröter, J., Samuels, B. L., Treguier, A.-M., Toggweiler, J. R., Tsujino, H., Vallis, G. K., & White, L. (2010). Problems and prospects in large-scale ocean circulation models. In J. Hall, D. Harrison, & D. Stammer (Eds.), *Proceedings of the OceanObs09 Conference: Sustained Ocean Observations and Information for Society, Venice, Italy, 21-25 September 2009*. ESA Publication WPP-306 volume 2.
- Griffies, S. M., Biastoch, A., Böning, C. W., Bryan, F., Danabasoglu, G., Chassignet, E., England, M. H., Gerdes, R., Haak, H., Hallberg, R. W., Hazeleger, W., Jungclaus, J., Large, W. G., Madec, G., Pirani, A., Samuels, B. L., Scheinert, M., Gupta, A. S., Severijns, C. A., Simmons, H. L., Treguier, A. M., Winton, M., Yeager, S., & Yin, J. (2009). Coordinated Ocean-ice Reference Experiments (COREs). *Ocean Modelling*, 26, 1–46.
- Griffies, S. M., Böning, C. W., Bryan, F. O., Chassignet, E. P., Gerdes, R., Hasumi, H., Hirst, A., Treguier, A.-M., & Webb, D. (2000a). Developments in ocean climate modelling. *Ocean Modelling*, 2, 123–192.

- 1505 Griffies, S. M., & Greatbatch, R. J. (2012). Physical processes that impact the evolution  
1506 of global mean sea level in ocean climate models. *Ocean Modelling*, 51, 37–72.
- 1507 Griffies, S. M., & Hallberg, R. W. (2000). Biharmonic friction with a Smagorinsky  
1508 viscosity for use in large-scale eddy-permitting ocean models. *Monthly Weather*  
1509 *Review*, 128, 2935–2946.
- 1510 Griffies, S. M., Pacanowski, R., Schmidt, M., & Balaji, V. (2001). Tracer conservation  
1511 with an explicit free surface method for z-coordinate ocean models. *Monthly Weather*  
1512 *Review*, 129, 1081–1098.
- 1513 Griffies, S. M., Pacanowski, R. C., & Hallberg, R. W. (2000b). Spurious diapycnal  
1514 mixing associated with advection in a z-coordinate ocean model. *Monthly Weather*  
1515 *Review*, 128, 538–564.
- 1516 Griffies, S. M., Winton, M., Donner, L. J., Downes, S. M., Farneti, R., Gnanadesikan,  
1517 A., Horowitz, L. W., Hurlin, W. J., Lee, H.-C., Liang, Z., Palter, J. B., Samuels,  
1518 B. L., Wittenberg, A. T., Wyman, B. L., Yin, J., & Zadeh, N. T. (2011). GFDL's  
1519 CM3 coupled climate model: Characteristics of the ocean and sea ice simulations.  
1520 *Journal of Climate*, 24, 3520–3544.
- 1521 Grinstein, F. F., Margolin, L. G., & Rider, W. J. (2007). A rationale for implicit LES.  
1522 In F. Grinstein, L. Margolin, & W. Rider (Eds.), *Implicit Large Eddy Simulation:*  
1523 *Computing Turbulent Fluid Dynamics*. Cambridge University Press.
- 1524 Grist, J. P., Josey, S. A., Marsh, R., Good, S. A., Coward, A., de Cuevas, B., Alderson,  
1525 S., New, A., & Madec, G. (2010). The roles of surface heat flux and ocean heat  
1526 transport convergence in determining Atlantic Ocean temperature variability. *Ocean*  
1527 *Dynamics*, 60, 771–790.
- 1528 Hall, A., & Manabe, S. (1997). Can local, linear stochastic theory explain sea surface  
1529 temperature and salinity variability? *Climate Dynamics*, 13, 167–180.
- 1530 Hallberg, R. W. (2003). The suitability of large-scale ocean models for adapting pa-  
1531 rameterizations of boundary mixing and a description of a refined bulk mixed layer  
1532 model. In P. Müller, & C. Garrett (Eds.), *Near-Boundary Processes and Their Pa-*  
1533 *rameterization* Proceedings of the 13th 'Aha Huliko'a Hawaiian Winter Workshop  
1534 (pp. 187–203). University of Hawaii at Manoa.
- 1535 Haney, R. L. (1971). Surface thermal boundary conditions for ocean circulation mod-  
1536 els. *Journal of Physical Oceanography*, 1, 241–248.
- 1537 Haney, R. L. (1991). On the pressure gradient force over steep topography in sigma-  
1538 coordinate ocean models. *Journal of Physical Oceanography*, 21, 610–619.
- 1539 Hasselmann, K. (1976). Stochastic climate models. Part I: Theory. *Tellus*, 28, 473–485.
- 1540 Herzfeld, M., Schmidt, M., Griffies, S. M., & Liang, Z. (2011). Realistic test cases for  
1541 limited area ocean modelling. *Ocean Modelling*, 37, 1–34.

- 1542 Hesselberg, T. (1926). Die Gesetze der ausgeglichenen atmosphaerischen Bewegun-  
1543 gen. *Beitrageder Physik der freien Atmosphere*, 12, 141–160.
- 1544 Hill, C., Ferreira, D., Campin, J.-M., Marshall, J., Abernathey, R., & Barrier, N. (2012).  
1545 Controlling spurious diapyncal mixing in eddy-resolving height-coordinate ocean  
1546 models–insights from virtual deliberate tracer release experiments. *Ocean Mod-*  
1547 *elling*, 45–46, 14–26.
- 1548 Hofmann, M., & Morales-Maqueda, M. (2011). The response of Southern Ocean ed-  
1549 dies to increased midlatitude westerlies: A non-eddy resolving model study. *Geo-*  
1550 *physical Research Letters*, 38 (L03605), doi:10.1029/2010GL045972.
- 1551 Holland, W. R., & Rhines, P. B. (1980). An example of eddy-induced ocean circulation.  
1552 *Journal of Physical Oceanography*, 10, 1010–1031.
- 1553 Holloway, G. (1986). Eddies, waves, circulation, and mixing: statistical geofluid me-  
1554 chanics. *Annual Review of Fluid Mechanics*, 18, 91–147.
- 1555 Holloway, G. (1989). Subgridscale representation. In D. L. Anderson, & J. Willebrand  
1556 (Eds.), *Oceanic Circulation Models: Combining Data and Dynamics* (pp. 513–593).  
1557 Kluwer Academic Publishers volume 284 of *NATO ASI Series. Series C*.
- 1558 Holloway, G. (1992). Representing topographic stress for large-scale ocean models.  
1559 *Journal of Physical Oceanography*, 22, 1033–1046.
- 1560 Huang, R. X., Jin, X., & Zhang, X. (2001). An oceanic general circulation model in  
1561 pressure coordinates. *Advances in Atmospheric Physics*, 18, 1–22.
- 1562 Hughes, C. (2002). Zonal jets in and near the Coral Sea seen by satellite altimetry.  
1563 *Geophysical Research Letters*, 29, 1330.
- 1564 Ilicak, M., Adcroft, A. J., Griffies, S. M., & Hallberg, R. W. (2012). Spurious di-  
1565 aneutral mixing and the role of momentum dissipation. *Ocean Modelling*, 45–46,  
1566 37–58.
- 1567 Illig, S., Dewitte, B., Ayoub, N., du Penhoat, Y., abd P. De Mey, G. R., Bonjean, F., &  
1568 Lagerloef, G. S. E. (2004). Interannual long equatorial waves in the tropical Atlantic  
1569 from a high-resolution ocean general circulation model experiment in 1981–2000.  
1570 *Journal of Geophysical Research*, 109-C02022, doi:10.1029/2003JC001771.
- 1571 IOC, SCOR, & IAPSO (2010). *The international thermodynamic equation of*  
1572 *seawater-2010: calculation and use of thermodynamic properties*. available from  
1573 <http://www.TEOS-10.org>; Intergovernmental Oceanographic Commission, Manuals  
1574 and Guides No. 56, UNESCO. 196pp.
- 1575 Iudicone, D., Madec, G., & McDougall, T. J. (2008). Water-mass transformations in a  
1576 neutral density framework and the key role of light penetration. *Journal of Physical*  
1577 *Oceanography*, 38, 1357–1376.

- 1578 Iudicone, D., Rodgers, K., Stendardo, I., Aumont, O., Madec, G., Bopp, L., Mangoin,  
1579 O., & d'Alcala, M. R. (2011). Water masses as a unifying framework for under-  
1580 standing the Southern Ocean Carbon Cycle. *Biogeosciences*, 8, 1031–1052.
- 1581 Jackson, L., Hallberg, R., & Legg, S. (2008). A parameterization of shear-driven turbu-  
1582 lence for ocean climate models. *Journal of Physical Oceanography*, 38, 1033–1053.
- 1583 Jiang, C., Thompson, L., & Kelly, K. (2008). Equatorial influence of QuikSCAT winds  
1584 in an isopycnal ocean model compared to NCEP2 winds. *Ocean Modelling*, 24,  
1585 65–71.
- 1586 Jochum, M., , Danabasoglu, G., Holland, M., Kwon, Y.-O., & Large, W. (2008).  
1587 Ocean viscosity and climate. *Journal of Geophysical Research*, 114 C06017,  
1588 doi:10.1029/2007JC004515.
- 1589 Jochum, M. (2009). Impact of latitudinal variations in vertical diffusivity  
1590 on climate simulations. *Journal of Geophysical Research*, 114 C01010,  
1591 doi:10.1029/2008JC005030.
- 1592 Jones, H., & Marshall, J. (1993). Convection with rotation in a neutral ocean: a study  
1593 of open-ocean deep convection. *Journal of Physical Oceanography*, 23, 1009–1039.
- 1594 Jongma, J., Driesschaert, E., Fichet, T., Goosse, H., & Renssen, H. (2009). The  
1595 effect of dynamic-thermodynamic icebergs on the Southern Ocean climate in a three-  
1596 dimensional model. *Ocean Modelling*, 26, 104–113.
- 1597 Khairoutdinov, M., DeMott, C., & Randall, D. (2008). Evaluation of the simulated  
1598 interannual and subseasonal variability in an AMIP-style simulation using the CSU  
1599 Multiscale Modeling Framework. *Journal of Climate*, 21, 413–431.
- 1600 Killworth, P. D., & Edwards, N. (1999). A turbulent bottom boundary layer code for  
1601 use in numerical ocean models. *Journal of Physical Oceanography*, 29, 1221–1238.
- 1602 Killworth, P. D., Smeed, D., & Nurser, A. (2000). The effects on ocean models of  
1603 relaxation toward observations at the surface. *Journal of Physical Oceanography*,  
1604 30, 160–174.
- 1605 Kitsios, V., Frederiksen, J. S., & Zidikheri, M. J. (2013). Scaling laws for parame-  
1606 terisations of subgrid eddy-eddy interactions in simulations of oceanic circulations.  
1607 *Ocean Modelling*, ..., doi.org/10.1016/j.ocemod.2013.05.001.
- 1608 Klein, P., & Lapeyre, G. (2009). The oceanic vertical pump induced by mesoscale and  
1609 submesoscale turbulence. *Annual Reviews of Marine Science*, 1, 351–375.
- 1610 Klinger, B. A., Marshall, J., & Send, U. (1996). Representation of convective plumes  
1611 by vertical adjustment. *Journal of Geophysical Research*, 101, 18175–18182.
- 1612 Klocker, A., & McDougall, T. J. (2010). Influence of the nonlinear equation of state on  
1613 global estimates of diapycnal advection and diffusion. *Journal of Physical Oceanog-  
1614 raphy*, 40, 1690–1709.

- 1615 Koch-Larrouy, A., Madec, G., Blanke, B., & Molcard, R. (2008). Water mass trans-  
1616 formation along the Indonesian throughflow in an OGCM. *Journal of Physical*  
1617 *Oceanography*, 58, 289–309.
- 1618 Kopp, R. E., Mitrovica, J. X., Griffies, S. M., Yin, J., Hay, C. C., & Stouffer, R. J.  
1619 (2010). The impact of Greenland melt on regional sea level: a preliminary com-  
1620 parison of dynamic and static equilibrium effects. *Climatic Change Letters*, 103,  
1621 619–625.
- 1622 Kuhlbrodt, T., Griesel, A., Montoya, M., Levermann, A., Hofmann, M., & Rahmstorf,  
1623 S. (2007). On the driving processes of the Atlantic meridional overturning circula-  
1624 tion. *Reviews of Geophysics*, 45, doi:10.1029/2004RG000166.
- 1625 Kunze, E., Firing, E., Hummon, J. M., Chereskin, T. K., & Thurnherr, A. M. (2006).  
1626 Global Abyssal Mixing Inferred from Lowered ADCP Shear and CTD Strain Pro-  
1627 files. *Journal of Physical Oceanography*, 36, 1553–1576.
- 1628 Kunze, E., & Sanford, T. B. (1996). Abyssal mixing: where it is not. *Journal of*  
1629 *Physical Oceanography*, 26, 2286–2296.
- 1630 Laanaia, N., Wirth, A., Molines, J., Barnier, B., & Verron, J. (2010). On the numerical  
1631 resolution of the bottom layer in simulations of oceanic gravity currents. *Ocean*  
1632 *Science*, 6, 563–572.
- 1633 Large, W., McWilliams, J., & Doney, S. (1994). Oceanic vertical mixing: a review and  
1634 a model with a nonlocal boundary layer parameterization. *Reviews of Geophysics*,  
1635 32, 363–403.
- 1636 Large, W., & Yeager, S. (2004). Diurnal to decadal global forcing for ocean and sea-ice  
1637 models: the data sets and flux climatologies. NCAR Technical Note: NCAR/TN-  
1638 460+STR. CGD Division of the National Center for Atmospheric Research.
- 1639 Large, W. B., & Nurser, A. G. (2001). Ocean surface water mass transformation. In  
1640 G. Seidler, J. Church, & J. Gould (Eds.), *Ocean Circulation and Climate* (pp. 317–  
1641 336). San Diego: Academic Press volume 77 of *International Geophysics Series*.
- 1642 Large, W. G., Danabasoglu, G., Doney, S. C., & McWilliams, J. C. (1997). Sensitivity  
1643 to surface forcing and boundary layer mixing in a global ocean model: annual-mean  
1644 climatology. *Journal of Physical Oceanography*, 27, 2418–2447.
- 1645 Large, W. G., Danabasoglu, G., McWilliams, J. C., Gent, P. R., & Bryan, F. O. (2001).  
1646 Equatorial circulation of a global ocean climate model with anisotropic horizontal  
1647 viscosity. *Journal of Physical Oceanography*, 31, 518–536.
- 1648 Large, W. G., & Yeager, S. (2009). The global climatology of an interannually varying  
1649 air-sea flux data set. *Climate Dynamics*, 33, 341–364.
- 1650 Le Sommer, J., Penduff, T., Theetten, S., Madec, G., & Barnier, B. (2009). How mo-  
1651 mentum advection schemes influence current-topography interactions at eddy per-  
1652 mitting resolution. *Ocean Modelling*, 29, 1–14.



- 1653 Le Traon, P.-Y., Nadal, F., & Ducet, N. (1998). An improved mapping method of multi-  
1654 satellite altimeter data. *Journal of Atmospheric and Oceanic Technology*, 15, 522–  
1655 534.
- 1656 Leclair, M., & Madec, G. (2011).  $\tilde{z}$ -coordinate, an arbitrary Lagrangian-Eulerian coordinate  
1657 separating high and low frequency motions. *Ocean Modelling*, 37, 139–152.
- 1658 Ledwell, J. R., St-Laurent, L., Girton, J., & Toole, J. (2011). Diapycnal mixing in the  
1659 Antarctic Circumpolar Current. *Journal of Physical Oceanography*, 41, 241–246.
- 1660 Ledwell, J. R., & Watson, A. J. (1998). Mixing of a tracer in the pycnocline. *Journal*  
1661 *of Geophysical Research*, 103, 21499–21529.
- 1662 Ledwell, J. R., Watson, A. J., & Law, C. S. (1993). Evidence for slow mixing across the  
1663 pycnocline from an open-ocean tracer-release experiment. *Nature*, 364, 701–703.
- 1664 Legg, S. (2012). Overflows and convectively driven flows. In E. Chassignet,  
1665 C. Cenedese, & J. Verron (Eds.), *Buoyancy-Driven flows*. Cambridge UK: Cam-  
1666 bridge University Press.
- 1667 Legg, S., Briegleb, B., Chang, Y., Chassignet, E. P., Danabasoglu, G., Ezer, T., Gor-  
1668 don, A. L., Gries, S. M., Hallberg, R. W., Jackson, L., Large, W., Özgökmen, T. M.,  
1669 Peters, H., Price, J., Riemenschneider, U., Wu, W., Xu, X., & Yang, J. (2009). Im-  
1670 proving oceanic overflow representation in climate models: The Gravity Current En-  
1671 trainment Climate Process Team. *Bulletin of the American Meteorological Society*,  
1672 90, 657–670.
- 1673 Legg, S., Hallberg, R., & Girton, J. (2006). Comparison of entrainment in overflows  
1674 simulated by  $z$ -coordinate, isopycnal and non-hydrostatic models. *Ocean Modelling*,  
1675 11, 69–97.
- 1676 Legg, S., Jackson, L., & Hallberg, R. (2008). Eddy-resolving modeling of overflows.  
1677 In M. Hecht, & H. Hasumi (Eds.), *Eddy resolving ocean models* Geophysical Mono-  
1678 graph 177 (pp. 63–82). American Geophysical Union.
- 1679 Leith, C. E. (1996). Stochastic models of chaotic systems. *Physica D*, 98, 481–491.
- 1680 Lemarié, F., Debreu, L., Shchepetkin, A. F., & McWilliams, J. C. (2012a). On the  
1681 stability and accuracy of the harmonic and biharmonic isoneutral mixing operators  
1682 in ocean models. *Ocean Modelling*, 52–53, 9–35.
- 1683 Lemarié, F., Kurian, J., Shchepetkin, A. F., Molemaker, M. J., Colas, F., &  
1684 McWilliams, J. C. (2012b). Are there inescapable issues prohibiting the use of  
1685 terrain-following coordinates in climate models? *Ocean Modelling*, 42, 57–79.
- 1686 Lique, C., Treguier, A.-M., Scheinert, M., & Penduff, T. (2009). A model-based study  
1687 of ice and freshwater transport variability along both sides of Greenland. *Climate*  
1688 *Dynamics*, 33, 685–705.

- 1689 Lombard, A., Garric, G., & Penduff, T. (2009). Regional patterns of observed sea level  
1690 change: insights from a  $1/4^\circ$  global ocean/sea-ice hindcast. *Ocean Dynamics*, 59,  
1691 433–449.
- 1692 MacKinnon, J., Alford, M., Bouruet-Aubertot, P., Bindoff, N., Elipot, S., Gille, S.,  
1693 Girton, J., Gregg, M., Kunze, E., Naveira Garabato, A., Phillips, H., Pinkel, R.,  
1694 Polzin, K., Sanford, T., Simmons, H., & Speer, K. (2010). Using global arrays  
1695 to investigate internal-waves and mixing. In J. Hall, D. Harrison, & D. Stammer  
1696 (Eds.), *Proceedings of the OceanObs09 Conference: Sustained Ocean Observations  
1697 and Information for Society, Venice, Italy, 21-25 September 2009*. ESA Publication  
1698 WPP-306 volume 2.
- 1699 Maltrud, M., & McClean, J. (2005). An eddy resolving global  $1/10^\circ$  ocean simulation.  
1700 *Ocean Modelling*, 8, 31–54.
- 1701 Manizza, M., Le Quere, C., Watson, A., & Buitenhuis, E. (2005). Bio-optical feed-  
1702 backs among phytoplankton, upper ocean physics and sea-ice in a global model.  
1703 *Geophysical Research Letters*, 32, doi:10.1029/2004GL020778.
- 1704 Maqueda, M. M., & Holloway, G. (2006). Second-order moment advection scheme  
1705 applied to Arctic Ocean simulation. *Ocean Modelling*, 14, 197–221.
- 1706 Marchesiello, J. M. P., Debreu, L., & Couvelard, X. (2009). Spurious diapycnal mix-  
1707 ing in terrain-following coordinate models: The problem and a solution. *Ocean  
1708 Modelling*, 26, 156–169.
- 1709 Marchesiello, P., McWilliams, J., & Shchepetkin, A. (2001). Open boundary conditions  
1710 for long-term integration of regional oceanic models. *Ocean Modelling*, 3, 1–20.
- 1711 Margolin, L., Rider, W., & Grinstein, F. (2006). Modeling turbulent flow with implicit  
1712 LES. *Journal of Turbulence*, 7, 1–27.
- 1713 Marsh, R. (2000). Cabbeling due to isopycnal mixing in isopycnic coordinate models.  
1714 *Journal of Physical Oceanography*, 30, 1757–1775.
- 1715 Marshall, J., Adcroft, A., Campin, J.-M., Hill, C., & White, A. (2004). Atmosphere-  
1716 ocean modeling exploiting fluid isomorphisms. *Monthly Weather Review*, 132,  
1717 2882–2894.
- 1718 Marshall, J., Hill, C., Perelman, L., & Adcroft, A. (1997). Hydrostatic, quasi-  
1719 hydrostatic, and nonhydrostatic ocean modeling. *Journal of Geophysical Research*,  
1720 102, 5733–5752.
- 1721 Marshall, J., Jamous, D., & Nilsson, J. (1999). Reconciling thermodynamic and dy-  
1722 namic methods of computation of water-mass transformation rates. *Deep-Sea Re-  
1723 search I*, 46, 545–572.
- 1724 Marshall, J., & Schott, F. (1999). Open-ocean convection: observations, theory, and  
1725 models. *Reviews of Geophysics*, 37, 1–64.

- 1726 Martin, T., & Adcroft, A. (2010). Parameterizing the fresh-water flux from land ice to  
1727 ocean with interactive icebergs in a coupled climate model. *Ocean Modelling*, 34,  
1728 111–124.
- 1729 Maze, G., Forget, G., Buckley, M., Marshall, J., & Cerovecki, I. (2009). Using trans-  
1730 formation and formation maps to study the role of air-sea heat fluxes in the North  
1731 Atlantic eighteen degree water formation. *Journal of Physical Oceanography*, 39,  
1732 1818–1835.
- 1733 McDougall, T. J. (1987). Thermobaricity, cabbeling, and water-mass conversion. *Jour-  
1734 nal of Geophysical Research*, 92, 5448–5464.
- 1735 McDougall, T. J. (2003). Potential enthalpy: a conservative oceanic variable for evalu-  
1736 ating heat content and heat fluxes. *Journal of Physical Oceanography*, 33, 945–963.
- 1737 McDougall, T. J., Greatbatch, R., & Lu, Y. (2002). On conservation equations in  
1738 oceanography: How accurate are Boussinesq ocean models? *Journal of Physical  
1739 Oceanography*, 32, 1574–1584.
- 1740 McDougall, T. J., & McIntosh, P. C. (2001). The temporal-residual-mean velocity.  
1741 Part II: isopycnal interpretation and the tracer and momentum equations. *Journal of  
1742 Physical Oceanography*, 31, 1222–1246.
- 1743 McWilliams, J. C., Danabasoglu, G., & Gent, P. R. (1996). Tracer budgets in the warm  
1744 water sphere. *Tellus Series A*, 48, 179–192.
- 1745 McWilliams, J. C., & Sullivan, P. (2001). Vertical mixing by Langmuir circulations.  
1746 *Spill Science and Technology Bulletin*, 6, 225–237.
- 1747 Meehl, G., Covey, C., Delworth, T., Latif, M., McAvaney, B., Mitchell, J., Stouffer, R.,  
1748 & Taylor, K. (2007). The WCRP CMIP3 multimodel dataset: A new era in climate  
1749 change research. *Bulletin of the American Meteorological Society*, 88, 1383–1394.
- 1750 Meehl, G., Gent, P. R., Arblaster, J., Otto-Bliesner, B., Brady, E., & Craig, A. (2001).  
1751 Factors that affect the amplitude of El Niño in global coupled climate models. *Cli-  
1752 mate Dynamics*, 17, 515–526.
- 1753 Megann, A., New, A., Blaker, A., & Sinha, B. (2010). The sensitivity of a coupled  
1754 climate model to its ocean component. *Journal of Climate*, 23, 5126–5150.
- 1755 Melet, A., Hallberg, R., Legg, S., & Polzin, K. (2013). Sensitivity of the Pacific Ocean  
1756 state to the vertical distribution of internal-tide driven mixing. *Journal of Physical  
1757 Oceanography*, (pp. doi:10.1175/JPO-D-12-055.1).
- 1758 Melet, A., Verron, J., Gourdeau, L., & Koch-Larrouy, A. (2011). Solomon Sea wa-  
1759 ter masses pathways to the equator and their modifications. *Journal of Physical  
1760 Oceanography*, 41, 810–826.
- 1761 Mellor, G. L., Oey, L.-Y., & Ezer, T. (1998). Sigma coordinate pressure gradient errors  
1762 and the seamount problem. *Journal of Atmospheric and Oceanic Technology*, 15,  
1763 1122–1131.

- 1764 Merryfield, W. J., & Scott, R. (2007). Bathymetric influence on mean currents in two  
1765 high resolution near-global ocean models. *Ocean Modelling*, 16, 76–94.
- 1766 Mitrovica, J. X., Tamisiea, M. E., Davis, J. L., & Milne, G. A. (2001). Recent mass  
1767 balance of polar ice sheets inferred from patterns of global sea-level change. *Nature*,  
1768 409, 1026–1029.
- 1769 Müller, P. (2006). *The Equations of Oceanic Motions*. (1st ed.). Cambridge: Cambridge  
1770 University Press. 302pp.
- 1771 Nakano, H., & Sugimotohara, N. (2002). Effects of bottom boundary layer parameteri-  
1772 zation on reproducing deep and bottom waters in a world ocean model. *Journal of*  
1773 *Physical Oceanography*, 32, 1209–1227.
- 1774 Naveira-Garabato, A., Polzin, K., King, B., Heywood, K., & Visbeck, M. (2004). Wid-  
1775 spread intense turbulent mixing in the Southern Ocean. *Science*, 303, 210–213.
- 1776 Olbers, D. J., Willebrand, J., & Eden, C. (2012). *Ocean Dynamics*. (1st ed.). Berlin,  
1777 Germany: Springer. 704 pages.
- 1778 Pacanowski, R. C. (1987). Effect of equatorial currents on surface stress. *Journal of*  
1779 *Physical Oceanography*, 17, 833–838.
- 1780 Pacanowski, R. C., & Gnanadesikan, A. (1998). Transient response in a  $z$ -level ocean  
1781 model that resolves topography with partial-cells. *Monthly Weather Review*, 126,  
1782 3248–3270.
- 1783 Palmer, T., & Williams, P. (2008). Stochastic physics and climate modelling. *Philo-*  
1784 *sophical Transactions of the Royal Society A*, 366, 2421–2427.
- 1785 Palter, J. B., Griffies, S. M., Galbraith, E. D., Gnanadesikan, A., Samuels, B. L., &  
1786 Klocker, A. (2013). The deep ocean buoyancy budget and its temporal variability.  
1787 *Journal of Climate*, submitted.
- 1788 Parkinson, C., & Washington, W. (1979). A large-scale numerical model of sea ice.  
1789 *Journal of Geophysical Research*, 84, 311–337.
- 1790 Pedlosky, J. (1987). *Geophysical Fluid Dynamics*. (2nd ed.). Berlin Heidelberg New  
1791 York: Springer-Verlag. 710 + xv pp.
- 1792 Penduff, T., Juza, M., Brodeau, L., Smith, G. C., Barnier, B., Molines, J. M., Treguier,  
1793 A. M., & Madec, G. (2010). Impact of global ocean model resolution on sea-level  
1794 variability with emphasis on interannual time scales. *Ocean Science*, 6, 269–284.
- 1795 Penduff, T., Sommer, J. L., Barnier, B., Treguier, A.-M., Molines, J.-M., & Madec, G.  
1796 (2007). Influence of numerical schemes on current-topography interactions in  $1/4^\circ$   
1797 global ocean simulations. *Ocean Science*, 3, 509–524.
- 1798 Philander, S. G. (1990). *El Niño, La Niña, and the Southern Oscillation*. Academic  
1799 Press.

- 1800 Polzin, K. L., Toole, J. M., Ledwell, J. R., & Schmitt, R. W. (1997). Spatial variability  
1801 of turbulent mixing in the abyssal ocean. *Science*, 276, 93–96.
- 1802 Prather, M. (1986). Numerical advection by conservation of second-order moments.  
1803 *Journal of Geophysical Research*, 91, 6671–6681.
- 1804 Price, J., & Yang, J. (1998). Marginal sea overflows for climate simulations. In E. P.  
1805 Chassignet, & J. Verron (Eds.), *Ocean Modeling and Parameterization* (pp. 155–  
1806 170). Kluwer volume 516 of *NATO ASI Mathematical and Physical Sciences Series*.
- 1807 Redi, M. H. (1982). Oceanic isopycnal mixing by coordinate rotation. *Journal of*  
1808 *Physical Oceanography*, 12, 1154–1158.
- 1809 Redler, R., & Böning, C. W. (1997). Effect of the overflows on the circulation in the  
1810 subpolar north atlantic: A regional model study. *Journal of Geophysical Research*,  
1811 102, 18529–18552.
- 1812 Reif, F. (1965). *Fundamentals of Statistical and Thermal Physics*. New York:  
1813 McGraw-Hill.
- 1814 Ringler, T., Petersen, M., Higdon, R. L., Jacobsen, D., Jones, P. W., & Maltrud, M.  
1815 (2013). A multi-resolution approach to global ocean modeling. *Ocean Modelling*,  
1816 ..., doi.org/10.1016/j.ocemod.2013.04.010.
- 1817 Rivin, I., & Tziperman, E. (1997). Sensitivity of air-sea fluxes to SST perturbations.  
1818 *Journal of Climate*, 11, 2431–2446.
- 1819 Roberts, M. J., & Marshall, D. (1998). Do we require adiabatic dissipation schemes in  
1820 eddy-resolving ocean models? *Journal of Physical Oceanography*, 28, 2050–2063.
- 1821 Roberts, M. J., & Wood, R. (1997). Topographic sensitivity studies with a Bryan-Cox-  
1822 type ocean model. *Journal of Physical Oceanography*, 27, 823–836.
- 1823 Rodgers, K., Blanke, B., Madec, G., Aumont, O., Ciais, P., & Dutay, J.-C. (2003).  
1824 Extratropical sources of Equatorial Pacific upwelling in an OGCM. *Geophysical*  
1825 *Research Letters*, 30, doi:10.1029/2002GL016003.
- 1826 Rosati, A., & Miyakoda, K. (1988). A general circulation model for upper ocean  
1827 simulation. *Journal of Physical Oceanography*, 18, 1601–1626.
- 1828 Röske, F. (2006). A global heat and freshwater forcing dataset for ocean models. *Ocean*  
1829 *Modelling*, 11, 235–297.
- 1830 Saunders, P., & King, B. (1995). Bottom currents derived from a shipborne ADCP on  
1831 WOCE cruise A11 in the South Atlantic. *Journal of Physical Oceanography*, 25,  
1832 329–347.
- 1833 Schiller, A., & Fiedler, R. (2007). Explicit tidal forcing in an ocean general circulation  
1834 model. *Geophysical Research Letters*, 34.

- 1835 Schmitt, R. W. (1994). Double diffusion in oceanography. *Annual Review of Fluid*  
1836 *Mechanics*, 26, 255–285.
- 1837 Shchepetkin, A., & McWilliams, J. (2002). A method for computing horizontal  
1838 pressure-gradient force in an ocean model with a non-aligned vertical coordinate.  
1839 *Journal of Geophysical Research*, 108, 35.1–35.34.
- 1840 Shchepetkin, A., & McWilliams, J. (2005). The regional oceanic modeling system  
1841 (ROMS): a split-explicit, free-surface, topography-following-coordinate oceanic  
1842 model. *Ocean Modelling*, 9, 347–404.
- 1843 Shchepetkin, A. F., & McWilliams, J. C. (1998). Quasi-monotone advection schemes  
1844 based on explicit locally adaptive dissipation. *Monthly Weather Review*, 126, 1541–  
1845 1580.
- 1846 Simmons, H. L., Jayne, S. R., St.Laurent, L. C., & Weaver, A. J. (2004). Tidally driven  
1847 mixing in a numerical model of the ocean general circulation. *Ocean Modelling*, 6,  
1848 245–263.
- 1849 Smagorinsky, J. (1993). Some historical remarks on the use of nonlinear viscosities. In  
1850 B. Galperin, & S. A. Orszag (Eds.), *Large Eddy Simulation of Complex Engineering*  
1851 *and Geophysical Flows* (pp. 3–36). Cambridge University Press.
- 1852 Smith, K. S. (2007). The geography of linear baroclinic instability in earth’s oceans.  
1853 *Journal of Marine Research*, 65, 655–683.
- 1854 Smith, K. S., & Vallis, G. K. (2001). The scales and equilibration of midocean eddies:  
1855 freely evolving flow. *Journal of Physical Oceanography*, 31, 554–570.
- 1856 Smith, R., Maltrud, M., Bryan, F., & Hecht, M. (2000). Numerical simulation of the  
1857 North Atlantic at  $1/10^\circ$ . *Journal of Physical Oceanography*, 30, 1532–1561.
- 1858 Smith, R. D., & McWilliams, J. C. (2003). Anisotropic horizontal viscosity for ocean  
1859 models. *Ocean Modelling*, 5, 129–156.
- 1860 Solomon, H. (1971). On the representation of isentropic mixing in ocean models.  
1861 *Journal of Physical Oceanography*, 1, 233–234.
- 1862 Speer, K., & Tziperman, E. (1992). Rates of water mass formation in the North Atlantic  
1863 Ocean. *Journal of Physical Oceanography*, 22, 2444–2457.
- 1864 Speich, S., Blanke, B., de Vries, P., Drijfhout, S., Döös, K., , Ganachaud, A., & Marsh,  
1865 R. (2002). Tasman leakage: A new route in the global ocean conveyor belt. *Gophys-*  
1866 *ical Research Letters*, 29.
- 1867 Stacey, M. W., Pond, S., & Nowak, Z. P. (1995). A numerical model of the circulation  
1868 in Knight Inlet, British Columbia, Canada. *Journal of Physical Oceanography*, 25,  
1869 1037–1062.
- 1870 Stammer, D. (1998). On eddy characteristics, eddy transports, and mean flow properties.  
1871 *Journal of Physical Oceanography*, 28, 727–739.

- 1872 Starr, V. P. (1945). A quasi-Lagrangian system of hydrodynamical equations. *Journal*  
1873 *of Meteorology*, 2, 227–237.
- 1874 Stewart, A., & Dellar, P. (2011). The role of the complete Coriolis force in cross-  
1875 equatorial flow of abyssal ocean currents. *Ocean Modelling*, 38, 187 – 202.
- 1876 Sullivan, P. P., & McWilliams, J. C. (2010). Dynamics of winds and currents coupled  
1877 to surface waves. *Annual Review of Fluid Mechanics*, 42, 19–42.
- 1878 Sullivan, P. P., McWilliams, J. C., & Melville, W. K. (2007). Surface gravity wave  
1879 effects in the oceanic boundary layer: large-eddy simulation with vortex force and  
1880 stochastic breakers. *Journal of Fluid Mechanics*, 593, 405–452.
- 1881 Tatebe, H., & Hasumi, H. (2010). Formation mechanism of the Pacific equatorial  
1882 thermocline revealed by a general circulation model with a high accuracy tracer  
1883 advection scheme. *Ocean Modelling*, 35, 245–252.
- 1884 Taylor, P. (2000). Final Report of the Joint WCRP/SCOR Working Group on Air-  
1885 Sea Fluxes: Intercomparison and validation of ocean-atmosphere energy flux fields.  
1886 WCRP-112, WMO/TD-No.1036 (p. 303pp). World Climate Research Programme.
- 1887 Timmermann, R., Danilov, S., Schröter, J., Böning, C., Sidorenko, D., & Rollenhagen,  
1888 K. (2009). Ocean circulation and sea ice distribution in a finite element global sea  
1889 ice-ocean model. *Ocean Modelling*, 27, 114–129.
- 1890 Toole, J. M., Schmitt, R. W., & Polzin, K. L. (1997). Near-boundary mixing above the  
1891 flanks of a mid-latitude seamount. *Journal of Geophysical Research*, 102, 947–959.
- 1892 Treguier, A., Barnier, B., Miranda, A., Molines, J., Grima, N., Imbard, M., Madec, G.,  
1893 Messenger, C., Reynaud, T., & Michel, S. (2001). An eddy-permitting model of the  
1894 Atlantic circulation: Evaluating open boundary conditions. *Journal of Geophysical*  
1895 *Research-oceans*, 106, 22115–22129.
- 1896 Treguier, A., Ferron, B., & Dussin, R. (2012). Buoyancy-driven currents in eddying  
1897 ocean models. In E. Chassignet, C. Cenedese, & J. Verron (Eds.), *Buoyancy-Driven*  
1898 *flows*. Cambridge UK: Cambridge University Press.
- 1899 Treguier, A. M. (1992). Kinetic energy analysis of an eddy resolving, primitive equa-  
1900 tion model of the North Atlantic. *Journal of Geophysical Research*, 97, 687–701.
- 1901 Treguier, A. M., Le Sommer, J., Molines, J. M., & de Cuevas, B. (2010). Response  
1902 of the Southern Ocean to the Southern Annular Mode: Interannual variability and  
1903 multidecadal trend. *Journal of Physical Oceanography*, 40, 1659–1668.
- 1904 Tziperman, E. (1986). On the role of interior mixing and air-sea fluxes in determining  
1905 the stratification and circulation in the oceans. *Journal of Physical Oceanography*,  
1906 16, 680–693.
- 1907 Vallis, G. K. (2006). *Atmospheric and Oceanic Fluid Dynamics: Fundamentals and*  
1908 *Large-scale Circulation*. (1st ed.). Cambridge: Cambridge University Press. 745 +  
1909 xxv pp.

- 1910 van Sebille, E., Jan van Leeuwen, P., Biastoch, A., Barron, C. N., & de Ruijter, W.  
1911 P. M. (2009). Lagrangian validation of numerical drifter trajectories using drifting  
1912 buoys: Application to the Agulhas system. *Ocean Modelling*, 29, 269–276.
- 1913 Veneziani, M., Griffa, A., Garraffo, Z., & Chassignet, E. (2005). Lagrangian spin pa-  
1914 rameter and coherent structures from trajectories released in a high-resolution ocean  
1915 model. *Journal of Marine Research*, 63, 753–788.
- 1916 Veronis, G. (1975). The role of models in tracer studies. In *Numerical Models of Ocean*  
1917 *Circulation*. National Academy of Sciences.
- 1918 Vialard, J., & Delecluse, P. (1998). An OGCM study for the TOGA decade. Part I:  
1919 Role of salinity in the physics of the Western Pacific Fresh Pool. *Journal of Physical*  
1920 *Oceanography*, 28, 1071–1088.
- 1921 Volkov, D., & Fu, L.-L. (2008). The role of vorticity fluxes in the dynamics of the  
1922 Zapiola Anticyclone. *Journal of Geophysical Research*, 113, C11015.
- 1923 Vries, P., & Döös, K. (2001). Calculating Lagrangian trajectories using time-dependent  
1924 velocity fields. *Journal of Atmospheric and Oceanic Technology*, 18, 1092–1101.
- 1925 Walin, G. (1982). On the relation between sea-surface heat flow and thermal circulation  
1926 in the ocean. *Tellus*, 34, 187–195.
- 1927 Webb, D. (2000). Evidence for shallow zonal jets in the South Equatorial Current  
1928 region of the Southwest Pacific. *Journal of Physical Oceanography*, 20, 706–720.
- 1929 Willebrand, J., Barnard, S., Barnier, B., Beckmann, A., Böning, C., Coulibaly, M.,  
1930 deCuevas, B., Dengg, J., Dieterich, C., Ernst, U., Herrmann, P., Jia, Y., Killworth,  
1931 P., Kröger, J., Lee, M.-M., Provost, C., Molines, J., New, A., Oschlies, A., Reynaud,  
1932 T., & West, L. (1997). *DYNAMO: Dynamics of North Atlantic Models: Simulation*  
1933 *and assimilation with high resolution models*. available from hdl:10013/epic.10757:  
1934 DYNAMO Scientific Report No 3.
- 1935 Williams, P. (2005). Modelling climate change: the role of unresolved processes.  
1936 *Philosophical Transactions of the Royal Society A*, 363, 2931–2946.
- 1937 Williams, R., Spall, M., & Marshall, J. (1995). Does Stommel’s mixed layer ‘demon’  
1938 work? *Journal of Physical Oceanography*, 25, 3089–3102.
- 1939 Winton, M., Hallberg, R., & Gnanadesikan, A. (1998). Simulation of density-  
1940 driven frictional downslope flow in z-coordinate ocean models. *Journal of Physical*  
1941 *Oceanography*, 28, 2163–2174.
- 1942 Wirth, A., & Barnier, B. (2006). Tilted convective plumes in numerical experiments.  
1943 *Ocean Modelling*, 12, 101–111.
- 1944 Wirth, A., & Barnier, B. (2008). Mean circulation and structures of tilted ocean deep  
1945 convection. *Journal of Physical Oceanography*, 38, 803–816.



- 1946 Wu, W., Danabasoglu, G., & Large, W. (2007). On the effects of parameterized  
1947 Mediterranean overflow on North Atlantic ocean circulation and climate. *Ocean*  
1948 *Modelling*, 19, 31–52.
- 1949 Wunsch, C. (1997). The vertical partition of oceanic horizontal kinetic energy and the  
1950 spectrum of global variability. *Journal of Physical Oceanography*, 27, 1770–1794.
- 1951 Wunsch, C., & Ferrari, R. (2004). Vertical mixing, energy, and the general circulation  
1952 of the ocean. *Annual Reviews of Fluid Mechanics*, 36, 281–314.
- 1953 Wunsch, C., & Stammer, D. (1995). The global frequency-wavenumber spectrum of  
1954 oceanic variability estimated from TOPEX/POSEIDON altimetric measurements.  
1955 *Journal of Geophysical Research*, 100, 24,895–24,910.
- 1956 Xu, Y., & Scott, R. B. (2008). Subtleties in forcing eddy resolving ocean models with  
1957 satellite wind data. *Ocean Modelling*, 20, 240–251.
- 1958 Young, W. R. (2012). An exact thickness-weighted average formulation of the Boussi-  
1959 nesq equations. *Journal of Physical Oceanography*, 42, 692–707.